

Mismatch in the Classification of Linear Subspaces: Sufficient Conditions for Reliable Classification

Jure Sokolić, *Student Member, IEEE*, Francesco Renna, *Member, IEEE*, Robert Calderbank, *Fellow, IEEE*, and Miguel R. D. Rodrigues, *Senior Member, IEEE*

Abstract—This paper considers the classification of linear subspaces with mismatched classifiers. In particular, we assume a model where one observes signals in the presence of isotropic Gaussian noise and the distribution of the signals conditioned on a given class is Gaussian with a zero mean and a low-rank covariance matrix. We also assume that the classifier knows only a mismatched version of the parameters of input distribution *in lieu* of the true parameters. By constructing an asymptotic low-noise expansion of an upper bound to the error probability of such a mismatched classifier, we provide sufficient conditions for reliable classification in the low-noise regime that are able to sharply predict the absence of a classification error floor. Such conditions are a function of the geometry of the true signal distribution, the geometry of the mismatched signal distributions as well as the interplay between such geometries, namely, the principal angles and the overlap between the true and the mismatched signal subspaces. Numerical results demonstrate that our conditions for reliable classification can sharply predict the behavior of a mismatched classifier both with synthetic data and in a real semi-supervised motion segmentation application.

Index Terms—Classification, mismatch, linear subspace, Maximum-a-Posteriori classifier, error floor.

I. INTRODUCTION

Signal classification is a fundamental task in various fields, including statistics, machine learning and computer vision. One often approaches this problem by leveraging the Bayesian inference paradigm, where one infers the signal class from signal samples or measurements based on a model of the joint distribution of the signal and signal classes [1].

Such joint distribution is typically inferred by relying on pre-labeled data sets.¹ However, in practical applications, the methods used to estimate the distributions from training data inevitably lead to signal models that are not perfectly matched to the true underlying one. This can be due to an insufficient number of labeled data, the noise in the pre-labeled data [2], [3], [4], or due to the non-stationary statistical behaviour [5].

It is therefore relevant to ask the question:

This paper was presented in part at the 2015 IEEE International Symposium on Information Theory.

The work of Jure Sokolić, Francesco Renna and Miguel R. D. Rodrigues was supported in part by EPSRC under grant EP/K033166/1. The work of Robert Calderbank was supported in part by AFOSR under grant FA 9550-13-1-0076 and by NGA under grant HM017713-1-0006.

J. Sokolić, F. Renna and M. R. D. Rodrigues are with the Department of Electronic and Electrical Engineering, University College London, United Kingdom (email: {jure.sokolic.13, f.renna, m.rodrigues}@ucl.ac.uk).

R. Calderbank is with the Department of Electrical and Computer Engineering, Duke University, NC, USA (email: robert.calderbank@duke.edu).

¹Such approach is generally known as *supervised learning* in the machine learning literature.

What is the impact that a mismatched classifier, i.e. a classifier that infers the signal classes based on an inaccurate model of the data distribution in lieu of the true underlying data distribution, has on classification performance?

We answer this question for the scenario where the data classes are constrained to lie approximately on a low-dimensional linear subspace embedded in the high-dimensional ambient space. Indeed, there are various problems in signal processing, image processing and computer vision that conform to such a model, some of which are:

- *Face Recognition*: It can be shown that, provided that the Lambertian reflectance assumption is verified, the set of images taken from the same subject under different lighting conditions can be well approximated by a low-dimensional linear subspace embedded in the high-dimensional space [6]. This is leveraged in several face recognition applications [7]–[9].
- *Motion Segmentation*: It can also be shown – under the assumption of the affine projection camera model – that the coordinates of feature points associated with rigidly moving objects through different video frames lie in a 4 dimensional linear space [10], [11], [12]. This is leveraged in [10] to design subspace clustering algorithms that can perform motion segmentation.
- In general, (affine) subspaces or unions of (affine) subspaces can also be used to model other data such as images of handwritten digits [13].

Our contributions include:

- We derive an upper bound to the error probability associated with the mismatched classifier for the case where the distribution of the signal in a given class is Gaussian with zero-mean and low-rank covariance matrix.
- We then derive sufficient conditions for reliable classification in the asymptotic low-noise regime. Such conditions are expressed in terms of the geometry of the true signal model, the geometry of the mismatched signal model and the interaction of these geometries (via the principal angles associated with the subspaces of the true and mismatched signal models as well as the dimension of the intersection of such subspaces).
- We finally provide a number of results, both with synthetic and real data, that show that our sufficient conditions for reliable classification are sharp. In particular, we also use our theoretical framework to determine the number of training samples needed to achieve reliable

classification in a semi-supervised motion segmentation application.

A. Related Work

The concept of model mismatch has been widely explored by the information theory and communication theory communities. For example, in lossless source coding problems, mismatch between the distribution used to encode the source and the true distribution is shown to lead to a compression rate penalty which is determined by the Kullback-Leibler (KL) distance between the mismatched and the true distributions [14].

In channel coding problems, mismatch has an impact on the reliable information transmission rate that has been characterized via inner and outer bounds to the achievable rate and error exponents of different channel models [15]–[19]. The problem of mismatched quantization is considered in [20].

The concept of mismatch has also been explored in the machine learning literature [5]. In particular, [5] studies the impact on classification performance of training sets consisting of biased samples of the true distribution, expressing classification error bounds as a function of the sample bias severity and type. The effect of label noise in the training sets is also considered in classification algorithms such as Support Vector Machines [3] and Logistic Regression classifiers [4]. See also [2] for an overview of the literature on classification in presence of label noise.

In the field of Compressed Sensing (CS), the effect of basis mismatch and sensing matrix mismatch on signal reconstruction has been studied in [21]–[23]. The authors in [21] consider reconstruction of continuous-time sinusoidal signals and show that the reconstruction error is bounded by norm of the difference between the true and the mismatched bases. The authors in [22] study the mismatch in CS from the perspective of basis perturbation and show that the stability of the basis pursuit reconstruction scales linearly with the norm of the perturbation. The authors in [23] provide the error bounds for the best k -term approximation of the sparse signal, which is bounded by the norm of basis perturbation matrix.

Signal classification and estimation using mismatched models is also considered in [24]–[27]. For example, [26] expresses bounds to the error probability in the presence of mismatch via the f -Divergence between the true and mismatched source distributions, and [27] expresses the mean-squared error penalty in presence of mismatch in terms of the derivative of the KL distance between the true and the mismatched distributions with respect to the decoder signal to noise ratio (SNR). In particular, the work in [26] is closely related to our work in the sense that it also establishes bounds to the error probability in the presence of mismatch. However, the bounds in [26] are not as sharp as our bounds because they fail to capture the presence or absence of an error floor in the asymptotic regime of low noise.

B. Organization

The remainder of this paper is organized as follows: Section II introduces the observation and signal models, the Mismatched Maximum-a-Posteriori (MMAP) classifier and

the geometrical quantities associated with the signal and the mismatched model that are essential for the description of the MMAP classifier performance. The upper bound to the error probability associated with the MMAP classifier and the asymptotic expansion, which provide sufficient conditions for reliable classification in the low-noise regime, are given in Section III. In Section IV the theoretical results are validated via numerical experiments. An application of the proposed bound in a semi-supervised learning application is given in Section V. The paper is concluded in Section VI. The proofs of the results are given in the Appendix.

C. Notation

We use the following notation in the sequel: matrices, column vectors and scalars are denoted by boldface upper-case letters (\mathbf{X}), boldface lower-case letters (\mathbf{x}) and italic letters (x), respectively. $\mathbf{I}_N \in \mathbb{R}^{N \times N}$ denotes the identity matrix and $\mathbf{0}_{M \times N} \in \mathbb{R}^{M \times N}$ denotes the zero matrix. The subscripts are omitted when the dimensions are clear from the context. \mathbf{e}_k denotes the k -th basis vector in \mathbb{R}^N . The transpose, rank and determinant operators are denoted as $(\cdot)^T$, $\text{rank}(\cdot)$ and $|\cdot|$, respectively. $\|\mathbf{x}\|$ denotes Euclidean norm of the vector \mathbf{x} and $\|\mathbf{X}\|_2$ denotes the spectral matrix norm of the matrix \mathbf{X} . The image of a matrix is denoted by $\text{im}(\cdot)$ and the kernel of a matrix is denoted by $\text{ker}(\cdot)$. The sum of subspaces \mathcal{A} and \mathcal{B} is denoted as $\mathcal{A} + \mathcal{B}$. $\log(\cdot)$ denotes the natural logarithm, and the multi-variate Gaussian distribution with the mean μ and covariance matrix Σ is denoted as $\mathcal{N}(\mu, \Sigma)$. We also use the following asymptotic notation: $f(x) = \mathcal{O}(g(x))$ if $\lim_{x \rightarrow \infty} \frac{f(x)}{g(x)} = c$, where $c > 0$, and $f(x) = o(g(x))$ if $\lim_{x \rightarrow \infty} \frac{f(x)}{g(x)} = 0$.

II. PROBLEM STATEMENT

We consider a standard observation model:

$$\mathbf{y} = \mathbf{x} + \mathbf{n} \quad (1)$$

where $\mathbf{y} \in \mathbb{R}^N$ represents the observation vector, $\mathbf{x} \in \mathbb{R}^N$ represents the signal vector and $\mathbf{n} \sim \mathcal{N}(\mathbf{0}, \sigma^2 \mathbf{I}) \in \mathbb{R}^N$ represents observation noise, where σ^2 denotes the noise variance per dimension.² We also assume that the signal $\mathbf{x} \in \mathbb{R}^N$ is drawn from a class $c \in \{1, \dots, C\}$ with prior probability $P(c = i) = p_i$, and that the distribution of the signal \mathbf{x} conditioned on a given class $c = i$ is Gaussian with mean zero and (possibly) low-rank covariance matrix $\Sigma_i \in \mathbb{R}^{N \times N}$, i.e.

$$\mathbf{x}|c = i \sim \mathcal{N}(\mathbf{0}, \Sigma_i), \quad (2)$$

with $\text{rank}(\Sigma_i) = r_i \leq N$. Therefore, conditioned on a given class $c = i$, the signal lies on the linear subspace spanned by the eigenvectors associated with the positive eigenvalues of the covariance matrix Σ_i .

The classification problem involves inferring the correct class label c associated with the signal \mathbf{x} from the signal observation \mathbf{y} . It is well known that the optimal classification

²This noise vector can also model the fact that data does not always lie exactly on a low-dimensional subspace but rather approximately on a low-dimensional subspace [13].

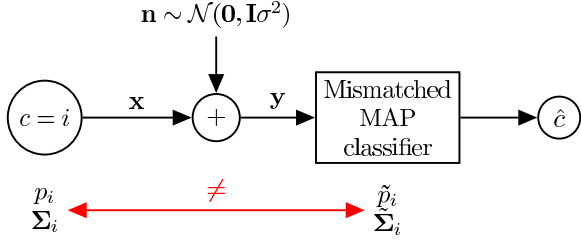


Fig. 1. System Model

rule, which minimizes the error probability, is given by the Maximum-A-Posteriori (MAP) classifier [1]:

$$\hat{c} = \arg \max_{i \in \{1, \dots, C\}} p(c = i | \mathbf{y}) = \arg \max_{i \in \{1, \dots, C\}} p(\mathbf{y} | c = i) p_i, \quad (3)$$

where $p(c = i | \mathbf{y})$ represents the *a posteriori* probability of class label $c = i$ given the observation \mathbf{y} and

$$p(\mathbf{y} | c = i) = \frac{1}{\sqrt{(2\pi)^N |\Sigma_i + \sigma^2 \mathbf{I}|}} e^{-\frac{1}{2} \mathbf{y}^T (\Sigma_i + \sigma^2 \mathbf{I})^{-1} \mathbf{y}} \quad (4)$$

represents the probability density function of the observation \mathbf{y} given the class label $c = i$.

However, we assume that the classifier does not have access to the true signal parameters p_i , $i = 1, \dots, C$ and Σ_i , $i = 1, \dots, C$ but rather to a set of mismatched parameters \tilde{p}_i , $i = 1, \dots, C$ and $\tilde{\Sigma}_i$, $i = 1, \dots, C$, where \tilde{p}_i is the mismatched *a priori* probability of the i -th class and $\tilde{\Sigma}_i$ is the mismatched covariance matrix associated with the class i with $\text{rank}(\tilde{\Sigma}_i) = \tilde{r}_i \leq N$.³ (See Fig. 1.)

Such a Mismatched-MAP (MMAP) classifier delivers the class estimate

$$\tilde{c} = \arg \max_{i \in \{1, \dots, C\}} \tilde{p}(c = i | \mathbf{y}) = \arg \max_{i \in \{1, \dots, C\}} \tilde{p}(\mathbf{y} | c = i) \tilde{p}_i, \quad (5)$$

where $\tilde{p}(c = i | \mathbf{y})$ denotes the mismatched *a posteriori* probability of class label $c = i$ given observation \mathbf{y} and

$$\tilde{p}(\mathbf{y} | c = i) = \frac{1}{\sqrt{(2\pi)^N |\tilde{\Sigma}_i + \sigma^2 \mathbf{I}|}} e^{-\frac{1}{2} \mathbf{y}^T (\tilde{\Sigma}_i + \sigma^2 \mathbf{I})^{-1} \mathbf{y}} \quad (6)$$

denotes the mismatched probability density function of the observation \mathbf{y} given the class label $c = i$.

The probability of error associated with a MMAP classifier is given by:

$$P(e) = \sum_{i=1}^C p_i \cdot P(e | c = i) \quad (7)$$

where

$$P(e | c = i) = \int_{-\infty}^{\infty} p(\mathbf{y} | c = i) \cdot u \left(\max_{\substack{j \\ j \neq i}} \log \left(\frac{\tilde{p}_j \tilde{p}(\mathbf{y} | c = j)}{\tilde{p}_i \tilde{p}(\mathbf{y} | c = i)} \right) \right) d\mathbf{y} \quad (8)$$

and $u(\cdot)$ is the unit-step function. This error probability cannot be calculated in closed form, but it can be easily bounded.

³We assume that C and σ^2 are known. Since we study the scenario where $\sigma^2 \rightarrow 0$, the assumption that σ^2 is known exactly is immaterial.

Our goal is to study the performance of the MMAP classifier by establishing conditions, which are a function of the geometry of the true and mismatched signal models as well as the interaction of such geometries, for reliable classification in the low-noise regime i.e. such that $\lim_{\sigma^2 \rightarrow 0} P(e) = 0$.

A. Geometrical Description of the Signals

Our characterization of the performance of the MMAP classifier will be expressed via various quantities that embody the geometry of the true signal model, the geometry of the mismatched signal model, and their interplay.

1) *Quantities associated with the geometry of the true signal model or the mismatched signal model:* We will consider a number of quantities that define the geometry of the true signal model or the geometry of the mismatched signal model:

- $\mathbf{U}_i \in \mathbb{R}^{N \times r_i}$ represents an orthonormal basis for $\text{im}(\Sigma_i)$ and $\tilde{\mathbf{U}}_i \in \mathbb{R}^{N \times \tilde{r}_i}$ represents an orthonormal basis for $\text{im}(\tilde{\Sigma}_i)$; these quantities follow directly from the truncated eigenvalue decompositions $\Sigma_i = \mathbf{U}_i \Lambda_i \mathbf{U}_i^T$ and $\tilde{\Sigma}_i = \tilde{\mathbf{U}}_i \tilde{\Lambda}_i \tilde{\mathbf{U}}_i^T$ where $\Lambda_i = \text{diag}(\lambda_1^i, \lambda_2^i, \dots, \lambda_{r_i}^i) \in \mathbb{R}^{r_i \times r_i}$ and $\tilde{\Lambda}_i = \text{diag}(\tilde{\lambda}_1^i, \tilde{\lambda}_2^i, \dots, \tilde{\lambda}_{\tilde{r}_i}^i) \in \mathbb{R}^{\tilde{r}_i \times \tilde{r}_i}$ are diagonal matrices containing the positive eigenvalues of Σ_i and $\tilde{\Sigma}_i$, respectively;
- $\tilde{\mathbf{U}}_{ij}^\cap \in \mathbb{R}^{N \times \tilde{r}_{ij}^\cap}$ represents an orthonormal basis for $\text{im}(\tilde{\Sigma}_i) \cap \text{im}(\tilde{\Sigma}_j)$, where \tilde{r}_{ij}^\cap is the dimension of the intersection $\text{im}(\tilde{\Sigma}_i) \cap \text{im}(\tilde{\Sigma}_j)$. $\tilde{\mathbf{U}}'_{ij} \in \mathbb{R}^{N \times \tilde{r}'_{ij}}$ represents an orthonormal basis for the orthogonal complement of $\text{im}(\tilde{\Sigma}_i) \cap \text{im}(\tilde{\Sigma}_j)$ in $\text{im}(\tilde{\Sigma}_i)$ and $\tilde{\mathbf{U}}'_{ji} \in \mathbb{R}^{N \times \tilde{r}'_{ji}}$ represents an orthonormal basis for the orthogonal complement of $\text{im}(\tilde{\Sigma}_i) \cap \text{im}(\tilde{\Sigma}_j)$ in $\text{im}(\tilde{\Sigma}_j)$ where \tilde{r}'_{ij} is the codimension of $\text{im}(\tilde{\Sigma}_i) \cap \text{im}(\tilde{\Sigma}_j)$ in $\text{im}(\tilde{\Sigma}_i)$ and \tilde{r}'_{ji} is the codimension of $\text{im}(\tilde{\Sigma}_i) \cap \text{im}(\tilde{\Sigma}_j)$ in $\text{im}(\tilde{\Sigma}_j)$; note that $\tilde{\mathbf{U}}_{ij}^\cap$ together with $\tilde{\mathbf{U}}'_{ij}$ and $\tilde{\mathbf{U}}'_{ji}$ complete the basis for $\text{im}(\tilde{\mathbf{U}}_i)$ and $\text{im}(\tilde{\mathbf{U}}_j)$, respectively, i.e. $\text{im}(\tilde{\mathbf{U}}_i) = \text{im}([\tilde{\mathbf{U}}_{ij}^\cap \tilde{\mathbf{U}}'_{ij}])$ and $\text{im}(\tilde{\mathbf{U}}_j) = \text{im}([\tilde{\mathbf{U}}'_{ij} \tilde{\mathbf{U}}'_{ji}])$.

2) *Quantities associated with the interplay between the geometry of the true signal model and the mismatched signal model:* We will also consider quantities that capture the interaction between the geometry of the true signal model and the geometry of the mismatched signal model:⁴

- $\mathbf{W}_{ij} \in \mathbb{R}^{N \times s_{ij}^W}$ represents an orthonormal basis for $\text{im}(\mathbf{U}_i) \cap \ker((\tilde{\mathbf{U}}'_{ij})^T)$ where $s_{ij}^W = \dim(\text{im}(\mathbf{U}_i) \cap \ker((\tilde{\mathbf{U}}'_{ij})^T))$;
- $\mathbf{V}_{ij} \in \mathbb{R}^{N \times s_{ij}^V}$ represents an orthonormal basis for the orthogonal complement of $\text{im}(\mathbf{U}_i) \cap \ker((\tilde{\mathbf{U}}'_{ij})^T)$ in $\text{im}(\mathbf{U}_i)$ where $s_{ij}^V = r_i - \dim(\text{im}(\mathbf{U}_i) \cap \ker((\tilde{\mathbf{U}}'_{ij})^T))$; then, $s_{ij}^V = \dim(\text{im}(\mathbf{V}_{ij})) = \text{rank}(\mathbf{V}_{ij})$ is the codimension of $\text{im}(\mathbf{W}_{ij})$ in $\text{im}(\mathbf{U}_i)$, or the number of linearly independent vectors in $\text{im}(\mathbf{V}_{ij})$.

3) *Principal angles and distance between subspaces:* Finally, our results will also be expressed via the principal angles between certain subspaces. In particular, consider a subspace \mathcal{Y} with an orthonormal basis $\mathbf{Y} \in \mathbb{R}^{N \times y}$, where $y = \dim(\mathcal{Y})$, and a subspace \mathcal{Z} with an orthonormal basis

⁴Note that $\text{im}([\mathbf{V}_{ij} \mathbf{W}_{ij}]) = \text{im}(\mathbf{U}_i)$.

$\mathbf{Z} \in \mathbb{R}^{N \times z}$, where $z = \dim(\mathcal{Z})$, and define $k = \min(y, z)$. Then the principal angles $0 \leq \theta_1 \leq \dots \leq \theta_k \leq \frac{\pi}{2}$ between \mathcal{Y} and \mathcal{Z} are given by the singular value decomposition (SVD):

$$\mathbf{Y}^T \mathbf{Z} = \mathbf{H} \mathbf{D} \mathbf{J}^T \quad (9)$$

where $\mathbf{H} \in \mathbb{R}^{y \times y}$ and $\mathbf{J} \in \mathbb{R}^{z \times z}$ are orthonormal matrices and $\mathbf{D} \in \mathbb{R}^{y \times z}$ is a rectangular diagonal matrix containing the singular values: $1 \geq d_1 \geq \dots \geq d_k \geq 0$. Each singular value d_l corresponds to the cosine of the principal angle θ_l between \mathcal{Y} and \mathcal{Z} , i.e., $d_l = \cos(\theta_l)$ [28].

The principal angles are used to define various distances on a Grassmann manifold [29]. We will be predominantly using the max correlation distance between two subspaces

$$d_{\max}(\mathcal{Y}, \mathcal{Z}) = d_{\max}(\mathbf{Y}, \mathbf{Z}) = \sin \theta_1 \quad (10)$$

which is a function of the smallest principal angle θ_1 , and the min correlation distance between two subspaces

$$d_{\min}(\mathcal{Y}, \mathcal{Z}) = d_{\min}(\mathbf{Y}, \mathbf{Z}) = \sin \theta_k \quad (11)$$

which is a function of the largest principal angle θ_k between the two subspaces. Note that we slightly abuse the notation in the second term of (10) and (11), as \mathbf{Y} and \mathbf{Z} are bases for the subspaces, not subspaces.

4) *Interpretation:* It is possible to cast some insight on the role of these various quantities in the characterization of the performance of the MMAP classifier.

Consider a two-class classification problem that involves distinguishing class 1 from class 2 in the low-noise regime (so $\mathbf{y} \approx \mathbf{x}$). It is clear that the MMAP classifier will associate an observation $\mathbf{y} \in \text{im}(\tilde{\mathbf{U}}'_{12})$ with class 1 and an observation $\mathbf{y} \in \text{im}(\tilde{\mathbf{U}}'_{21})$ with class 2; in turn, the MMAP classifier may associate an observation $\mathbf{y} \in \text{im}(\tilde{\mathbf{U}}'_{12})$ either with class 1 or 2. In general, the observation associated with class 1 is such that $\mathbf{y} \in \text{im}(\mathbf{U}_1) = \text{im}([\mathbf{V}_{12}, \mathbf{W}_{12}])$.

Assume however that the observation $\mathbf{y} | c = 1 \in \text{im}(\mathbf{W}_{12}) = \text{im}(\mathbf{U}_1) \cap \ker((\tilde{\mathbf{U}}'_{12})^T)$ ⁵, which implies that $\mathbf{y} \in \text{im}(\mathbf{U}_1)$ and also \mathbf{y} can be decomposed as the sum of a vector in $\ker((\tilde{\mathbf{U}}_1)^T)$ and a vector in $\text{im}(\tilde{\mathbf{U}}_1) \cap \text{im}(\tilde{\mathbf{U}}_2)$. Then, one would expect the relationship between subspaces $\text{im}(\mathbf{W}_{12})$ and $\ker((\tilde{\mathbf{U}}'_{21})^T)$ to play a role in the characterization of conditions for perfect classification in the low-noise regime. In fact, if $\mathbf{y} \notin \ker((\tilde{\mathbf{U}}'_{21})^T)$ then the MMAP classifier may associate \mathbf{y} to class 2 as illustrated in Fig. 2 (a) and Fig. 2 (b); in example (a) $\text{im}(\mathbf{W}_{12}) = \{0\} \subset \ker(\tilde{\mathbf{U}}'_{21}) = \mathbb{R}^2$ and $\text{im}(\mathbf{W}_{21}) = \text{im}(\mathbf{e}_2) \subseteq \ker(\tilde{\mathbf{U}}'_2) = \text{im}(\mathbf{e}_2)$, perfect classification in the low-noise regime is possible because the MMAP decision region associated with class 1 only captures signals from class 1 and likewise the MMAP decision region associated with class 2 only captures signals from class 2. On the other hand, in example (b), $\text{im}(\mathbf{W}_{12}) = \text{im}(\mathbf{e}_2) \not\subseteq \ker(\tilde{\mathbf{U}}'_{21}) = \text{im}(\mathbf{e}_1)$, and perfect classification in the low-noise regime is not possible: the MMAP decision region associated with class 1 only captures class 1 but the MMAP decision region associated with class 2 captures signals from class 1 and class 2.

⁵Note that $\ker((\tilde{\mathbf{U}}'_{ij})^T) = \ker((\tilde{\mathbf{U}}_i)^T) + \text{im}(\tilde{\mathbf{U}}'_{ij})$. See appendix.

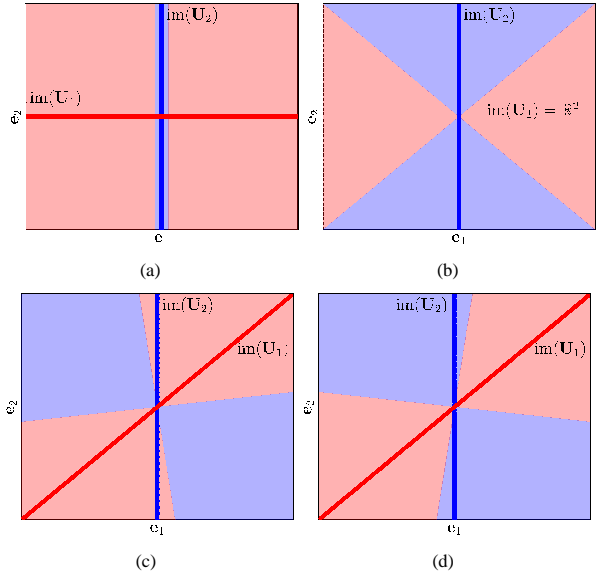


Fig. 2. The four plots illustrate the decision regions associated with the 2-class MMAP classifier for different values of \mathbf{U}_1 , \mathbf{U}_2 , $\tilde{\mathbf{U}}_1$ and $\tilde{\mathbf{U}}_2$ in the limit $\sigma^2 \rightarrow 0$. Transparent red and blue regions indicate the decision region where MMAP outputs class labels 1 and 2, respectively. Red line represent the signal subspaces $\text{im}(\mathbf{U}_1)$ and blue line represent the signal subspace $\text{im}(\mathbf{U}_2)$ (note that plot (b) does not have a red line since $\text{im}(\mathbf{U}_1) = \mathbb{R}^2$). In example (a) $\mathbf{U}_1 = \mathbf{e}_1$, $\tilde{\mathbf{U}}_1 = [\mathbf{e}_1, \mathbf{e}_2]$ and $\mathbf{U}_2 = \tilde{\mathbf{U}}_2 = \mathbf{e}_2$. In example (b) $\mathbf{U}_1 = [\mathbf{e}_1, \mathbf{e}_2]$, $\tilde{\mathbf{U}}_1 = \mathbf{e}_1$ and $\mathbf{U}_2 = \tilde{\mathbf{U}}_2 = \mathbf{e}_2$. In example (c) $\mathbf{U}_1 = \tilde{\mathbf{U}}_1 = [\cos(\frac{\pi}{4}), \sin(\frac{\pi}{4})]^T$, $\mathbf{U}_2 = \mathbf{e}_2$ and $\tilde{\mathbf{U}}_2 = [\cos(\frac{5\pi}{6}), \sin(\frac{5\pi}{6})]^T$. In example (d) $\mathbf{U}_1 = \tilde{\mathbf{U}}_1 = [\cos(\frac{\pi}{4}), \sin(\frac{\pi}{4})]^T$, $\mathbf{U}_2 = \mathbf{e}_2$ and $\tilde{\mathbf{U}}_2 = [\cos(\frac{4\pi}{6}), \sin(\frac{4\pi}{6})]^T$.

In contrast, assume now that the observation $\mathbf{y} \in \text{im}(\mathbf{V}_{12}) = \text{im}(\mathbf{U}_1) \cap (\text{im}(\tilde{\mathbf{U}}'_{12}) + \ker(\mathbf{U}_1^T))$. This implies that $\mathbf{y} \in \text{im}(\mathbf{U}_1)$ and $\mathbf{y} \perp \ker(\tilde{\mathbf{U}}_1^T)$ and $\mathbf{y} \perp \text{im}(\tilde{\mathbf{U}}_1) \cap \text{im}(\tilde{\mathbf{U}}_2)$. Therefore, in the low-noise regime, \mathbf{y} can be potentially associated to the correct class 1 depending on the distance (in an appropriate sense) between $\text{im}(\mathbf{V}_{12})$ and $\text{im}(\tilde{\mathbf{U}}'_{12})$ and the distance between $\text{im}(\mathbf{V}_{12})$ and $\text{im}(\tilde{\mathbf{U}}'_{21})$. This is illustrated in Fig. 2 (c) and Fig. 2 (d). In examples (c) and (d) the $\mathbf{V}_{ij} = \mathbf{U}_i$ and $\tilde{\mathbf{U}}'_{ij} = \tilde{\mathbf{U}}_i$, $i = 1, 2$. In case (c), the angle between $\text{im}(\mathbf{V}_{12})$ and $\tilde{\mathbf{U}}_2$ is smaller than the angle between $\text{im}(\mathbf{V}_{12})$ and $\tilde{\mathbf{U}}_1$, which leads to misclassification of signals from class 2. This is also indicated by the decision regions. In contrast, the angle between $\text{im}(\mathbf{V}_{12})$ and $\text{im}(\tilde{\mathbf{U}}_2)$ is larger than the angle between $\text{im}(\mathbf{V}_{12})$ and $\text{im}(\tilde{\mathbf{U}}_1)$ in example (d), which leads to perfect classification of signals from class 2 in the low noise regime.

The ensuing analysis shows how these various quantities – which are readily computed from the underlying geometry of the true subspaces and the mismatched ones – can be used as a proxy to define sufficient conditions for perfect classification in the low-noise regime. In particular, these quantities bypass the need to compute the decision regions associated with the MMAP classifier in order to quantify the performance.

III. CONDITIONS FOR RELIABLE CLASSIFICATION

We now consider (sufficient) conditions for reliable classification in the low-noise regime. We derive these conditions directly from a low-noise expansion of an upper bound to the error probability associated with the MMAP classifier.

The following upper bound to the probability of error associated with a MMAP classifier will play a key role in the analysis.

Theorem 1: Set $\alpha_{ij} > 0 \forall (i, j), i \neq j$. Set

$$\Sigma_{ij} = (\Sigma_i + \sigma^2 \mathbf{I})^{-1} + \alpha_{ij} (\tilde{\Sigma}_j + \sigma^2 \mathbf{I})^{-1} - \alpha_{ij} (\tilde{\Sigma}_i + \sigma^2 \mathbf{I})^{-1}. \quad (12)$$

Then the error probability associated with the MMAP classifier in (7) can be bounded as follows:

- If $\Sigma_{ij} \succ \mathbf{0} \forall (i, j)$ with $i \neq j$, then

$$P(e) \leq \bar{P}(e) = \sum_{i=1}^C p_i \cdot \left(\sum_{j=1, j \neq i}^C \bar{P}(e_{ij}) \right) \quad (13)$$

where

$$\bar{P}(e_{ij}) = \left(\frac{\tilde{p}_j}{\tilde{p}_i} \sqrt{\frac{|\tilde{\Sigma}_i + \sigma^2 \mathbf{I}|}{|\tilde{\Sigma}_j + \sigma^2 \mathbf{I}|}} \right)^{\alpha_{ij}} \cdot (|\Sigma_i + \sigma^2 \mathbf{I}| |\Sigma_{ij}|)^{-\frac{1}{2}}. \quad (14)$$

- If $\exists (i, j)$ with $i \neq j$: $\Sigma_{ij} \not\succ \mathbf{0}$ then

$$P(e) \leq \bar{P}(e) = 1. \quad (15)$$

Proof: The proof appears in Appendix. ■

This upper bound to the error probability of the MMAP classifier – in contrast with other bounds in the literature that always seem to exhibit an error floor [26], which is due to the fact that the bounds in [26] only account for the interplay between the true and mismatched models within a class whereas our bounds account for the interplay between the true and mismatched models both within a class and between classes. – can capture the fact that the error probability can tend to zero as the noise power also tends to zero, depending on the relation between the true signal parameters and the mismatched ones (see Section IV). This upper bound can also be tightened further by optimizing with respect to $\alpha_{ij} \forall i \neq j$.⁶

The following Theorem presents a low-noise expansion of the upper bound to the error probability of the MMAP classifier.

Theorem 2: The upper bound to the error probability of the MMAP classifier in (13) can be expanded as follows:

- Assume that $\forall (i, j), i \neq j$, the following conditions hold:

$$\text{im}(\mathbf{W}_{ij}) \subseteq \ker((\tilde{\mathbf{U}}'_{ji})^T) \quad (16)$$

$$\mathbf{V}_{ij}^T (\tilde{\mathbf{U}}'_{ij} (\tilde{\mathbf{U}}'_{ij})^T - \tilde{\mathbf{U}}'_{ji} (\tilde{\mathbf{U}}'_{ji})^T) \mathbf{V}_{ij} \succ \mathbf{0} \text{ or } s_{ij}^V = 0. \quad (17)$$

Then

- If $d \leq 0$:

$$\bar{P}(e) = \mathcal{O}(1), \quad \sigma^2 \rightarrow 0. \quad (18)$$

⁶Note that the optimization of $\alpha_{ij} \forall i \neq j$ for a given value of σ^2 is not trivial. However, such optimization is not relevant to determine whether the upper bound to the probability of error presents an error floor or not.

- If $d > 0$:

$$\bar{P}(e) = A \cdot (\sigma^2)^d + o\left((\sigma^2)^d\right), \quad \sigma^2 \rightarrow 0, \quad (19)$$

where $A > 0$,

$$d = \min_{(i \neq j)} d_{ij} \quad (20)$$

and

$$d_{ij} = \frac{1}{2} (s_{ij}^V + \alpha_{ij} (\tilde{r}_j - \tilde{r}_i)), \quad (21)$$

for any $\alpha_{ij} \in (0, \alpha_{ij}^0)$ where the value of α_{ij}^0 is given in the Appendix.

- Assume $\exists (i, j), i \neq j$, such that conditions (16) or (17) do not hold. Then

$$\bar{P}(e) = \mathcal{O}(1), \quad \sigma^2 \rightarrow 0. \quad (22)$$

Proof: The proof appears in Appendix. ■

The expansion of the upper bound to the error probability embodied in Theorem 2 provides a set of conditions, which are a function of the geometry of the true signal model, the geometry of the mismatched signal model, and the interaction of the geometries, that enable us to understand whether or not the upper bound to the error probability may exhibit an error floor. In particular, in view of the fact that we use the union bound in order to bound the error probability of a multi-class problem in terms of the error probabilities of two-class problems, these conditions have to hold for every pair of class labels $(i, j), i \neq j$. We can note that:

- The upper bound to the probability of error exhibits an error floor if either (16) or (17) are not satisfied for some pair $(i, j), i \neq j$. We have already seen that these conditions admit a simple interpretation (see Section II-A): note that both conditions (16) and (17) have to hold for a signal drawn from class i not to be assigned to class j in the low-noise regime; note also that the condition

$$\mathbf{V}_{ij}^T (\tilde{\mathbf{U}}'_{ij} (\tilde{\mathbf{U}}'_{ij})^T - \tilde{\mathbf{U}}'_{ji} (\tilde{\mathbf{U}}'_{ji})^T) \mathbf{V}_{ij} \succ \mathbf{0} \quad (23)$$

is also implied by

$$d_{\min}(\mathbf{V}_{ij}, \tilde{\mathbf{U}}'_{ij}) < d_{\max}(\mathbf{V}_{ij}, \tilde{\mathbf{U}}'_{ji}) \quad (24)$$

i.e. the largest principal angle between $\text{im}(\mathbf{V}_{ij})$ and $\text{im}(\tilde{\mathbf{U}}'_{ij})$ is required to be smaller than the smallest principal angle between $\text{im}(\mathbf{V}_{ij})$ and $\text{im}(\tilde{\mathbf{U}}'_{ji})$.⁷

- The upper bound to the probability of error does not exhibit an error floor if conditions (16) and (17) are satisfied for all pairs $(i, j), i \neq j$ and $d > 0$. In particular, necessary and sufficient conditions for $d > 0$ depend on the dimension of the various subspaces and their relation, i.e. $s_{ij}^V > 0$ for all pairs (i, j) such that $\tilde{r}_j - \tilde{r}_i \leq 0$ is necessary and sufficient for $d > 0$. For example, if the rank of all covariance matrices associated to the mismatched model is the same, i.e., if $\tilde{r}_i = \tilde{r}$, for $i = 1, \dots, C$, then $s_{ij}^V > 0, \forall (i, j), i \neq j$ is necessary and sufficient for $d > 0$. Note that a positive value for s_{ij}^V indicates that there is at least one vector in $\text{im}(\tilde{\mathbf{U}}_i)$ that is not contained

⁷The detailed derivation of this statement is reported in Appendix.

in $\ker((\tilde{\mathbf{U}}'_{ij})^T) = \ker(\tilde{\mathbf{U}}_i) + (\text{im}(\tilde{\mathbf{U}}_i) \cap \text{im}(\tilde{\mathbf{U}}_j))$, or equivalently, there is at least one vector in $\text{im}(\tilde{\mathbf{U}}_i)$ that has a non-zero projection onto $\text{im}(\tilde{\mathbf{U}}'_{ij})$, therefore leading to reliable classification of signals from class i .

- Note that parameters α_{ij} do not play a role in the characterization of the necessary and sufficient conditions for $d > 0$, in fact the conditions for $d_{ij} > 0$ do not depend on a particular value of α_{ij} , provided that $\alpha_{ij} \in (0, \frac{1}{|\tilde{r}_j - \tilde{r}_i|})$.
- Note also that the value of d represents a measure of robustness against noise in the low-noise regime, as it determines the speed at which the upper bound of the error probability decays with $1/\sigma^2$. In particular, higher values of d will represent higher robustness against noise, in the low-noise regime. For example, on assuming $\tilde{r}_i = \tilde{r}$ for $i = 1, \dots, C$, we observe that larger values of s_{ij}^V correspond to larger values of d . Therefore, as expected, higher levels of robustness are obtained when the overlap between $\text{im}(\mathbf{U}_i)$ and $\ker((\tilde{\mathbf{U}}'_{ij})^T) + \text{im}(\tilde{\mathbf{U}}_i) \cap \text{im}(\tilde{\mathbf{U}}_j)$, i.e. $\text{im}(\mathbf{W}_{ij})$, is reduced. In fact, as described in Section II-A, vectors in such spaces, i.e. $\mathbf{y} \in \text{im}(\mathbf{W}_{ij})$ may be associated with the wrong class j by the MMAP classifier.
- Note that the constant A in (19) distinguishes the upper bounds for different mismatched models with a constant d , in the low-noise regime, and is determined as the ratio of volumes of subspaces associated with true and mismatched signal subspaces and their interaction. See Appendix for the detailed expression.

Theorem 2 therefore leads immediately to sufficient conditions for reliable classification in the low-noise regime.

Corollary 1: If

$$\text{im}(\mathbf{W}_{ij}) \subseteq \ker((\tilde{\mathbf{U}}'_{ji})^T) \forall (i, j), i \neq j, \quad (25)$$

$$\mathbf{V}_{ij}^T (\tilde{\mathbf{U}}'_{ij} (\tilde{\mathbf{U}}'_{ij})^T - \tilde{\mathbf{U}}'_{ji} (\tilde{\mathbf{U}}'_{ji})^T) \mathbf{V}_{ij} \succ \mathbf{0} \forall (i, j), i \neq j \quad (26)$$

and $s_{ij}^V > 0 \forall (i, j)$ such that $\tilde{r}_j - \tilde{r}_i \leq 0$, then $\lim_{\sigma^2 \rightarrow 0} P(e) = 0$.

Proof: This follows directly from Theorem 1, since $\lim_{\sigma^2 \rightarrow 0} \bar{P}(e) = 0 \implies \lim_{\sigma^2 \rightarrow 0} P(e) = 0$. ■

Corollary 2: If

$$d_{\min}(\mathbf{U}_i, \tilde{\mathbf{U}}_i) < d_{\max}(\mathbf{U}_i, \tilde{\mathbf{U}}_j) \text{ and } s_{ij}^V > 0 \forall (i, j), i \neq j \quad (27)$$

then $\lim_{\sigma^2 \rightarrow 0} P(e) = 0$.

Proof: The proof appears in Appendix. ■

Note that the conditions in Corollary 2 are implied (hence are weaker) by the conditions in Corollary 1.

The conditions for reliable classification are particularly simple for the scenario where true and mismatched covariance matrices $\Sigma_i, \tilde{\Sigma}_i, i = 1, \dots, C$ are diagonal. In particular, it is straightforward to establish that

$$\text{im}(\mathbf{U}_i) \subseteq \ker((\tilde{\mathbf{U}}'_{ji})^T) \forall (i, j), i \neq j \quad (28)$$

and $s_{ij}^V > 0 \forall (i, j)$ such that $\tilde{r}_j - \tilde{r}_i \leq 0$ implies $\lim_{\sigma^2 \rightarrow 0} P(e) = 0$.

Note that in diagonal case the sufficient conditions for perfect classification simplify only to inclusion of subspaces.

In particular, recall that $\ker((\tilde{\mathbf{U}}'_{ji})^T)$ can be interpreted as a subspaces where signals are uniquely associated with class j . Condition (28) requires that signals from class i are not contained in this subspace.

We finally illustrate how our conditions cast insight onto the impact of mismatch for a two-class case where the mismatched subspaces are a rotated version of the true signal subspaces.

Example 1: Consider a two-class classification problem where $\mathbf{x}|c=1 \sim \mathcal{N}(\mathbf{0}, \mathbf{U}_1 \mathbf{U}_1^T)$ and $\mathbf{x}|c=2 \sim \mathcal{N}(\mathbf{0}, \mathbf{U}_2 \mathbf{U}_2^T)$ and

$$\tilde{\mathbf{U}}_1 = \mathbf{Q}_1 \mathbf{U}_1, \quad (29)$$

$$\tilde{\mathbf{U}}_2 = \mathbf{Q}_2 \mathbf{U}_2 \quad (30)$$

where $\mathbf{Q}_1 \in \mathbb{R}^{N \times N}$ and $\mathbf{Q}_2 \in \mathbb{R}^{N \times N}$ are orthogonal matrices, and $s_{12}, s_{21} > 0$.⁸ By defining

$$\epsilon_1 = \|\mathbf{I} - \mathbf{Q}_1\|_2, \quad \epsilon_2 = \|\mathbf{I} - \mathbf{Q}_2\|_2 \quad (31)$$

$$\delta_{12} = \max_l \cos \theta_l^{12} = \sqrt{1 - d_{\min}^2(\mathbf{U}_1, \mathbf{U}_2)}, \quad (32)$$

it follows that

$$1 - \delta_{12} > \epsilon_1 + \epsilon_2 \implies \lim_{\sigma^2 \rightarrow 0} P(e) = 0. \quad (33)$$

The proof is in the Appendix.

This example provides sufficient conditions for reliable classification in the low-noise regime by relating the degree of mismatch – measured in terms of the spectral norm of the matrix $\mathbf{I} - \mathbf{Q}_i$, $i = 1, 2$ – to the minimum principal angle between subspaces. It states that the larger the minimum principal angle between the spaces spanned by signals of class 1 and class 2, i.e. the larger $1 - \delta_{12}$, the more robust is the classifier against mismatch, where the level of mismatch is measured by $\epsilon_1 + \epsilon_2$. The maximum robustness against mismatch is obtained when $\delta_{12} = 0$, which means that signals from class 1 and class 2 are orthogonal.

This example also provides a rationale for state-of-the-art feature extraction mechanisms where the signal classes are transformed via a linear operator Φ prior to classification. In particular, assume that Σ_1 and Σ_2 correspond to the covariances of signals in class 1 and 2 after the transformation Φ : the example suggests that the operator Φ should transform the signal covariances so that δ_{12} is small (i.e. so that the signals from class 1 and 2 are close to orthogonal) in order to create robustness against mismatch. Such an approach is considered, for example, in [30], where signals are transformed by a matrix, which promotes large principal angles between the subspaces. Note that the work in [30] is not motivated on the basis of robustness against mismatch, but rather on intuitive insight about classification of signals that lie on subspaces.

IV. NUMERICAL RESULTS

We now show that our conditions for reliable classification in the low-noise regime are sharp, by revisiting the examples presented in Fig. 2 in Section II-A. The model parameters and results are summarized in Table 1.

⁸This condition insures that the mismatched subspaces are not completely orthogonal to the signal subspaces.

TABLE I
MISMATCH EXAMPLES GIVEN IN SECTION II-A.

	Model	Theory $\lim_{\sigma^2 \rightarrow 0} \bar{P}(e)$	Simulation $\lim_{\sigma^2 \rightarrow 0} P(e)$
(a)	$\mathbf{U}_1 = \mathbf{e}_1, \tilde{\mathbf{U}}_1 = [\mathbf{e}_1, \mathbf{e}_2], \mathbf{U}_2 = \tilde{\mathbf{U}}_2 = \mathbf{e}_2$	$= 0$	$= 0$
(b)	$\mathbf{U}_1 = [\mathbf{e}_1, \mathbf{e}_2], \tilde{\mathbf{U}}_1 = \mathbf{e}_1, \mathbf{U}_2 = \tilde{\mathbf{U}}_2 = \mathbf{e}_2$	> 0	> 0
(c)	$\mathbf{U}_1 = \tilde{\mathbf{U}}_1 = \cos\left(\frac{\pi}{4}\right)\mathbf{e}_1 + \sin\left(\frac{\pi}{4}\right)\mathbf{e}_2, \mathbf{U}_2 = \mathbf{e}_2, \tilde{\mathbf{U}}_2 = \cos\left(\frac{5\pi}{6}\right)\mathbf{e}_1 + \sin\left(\frac{5\pi}{6}\right)\mathbf{e}_2$	> 0	> 0
(c)	$\mathbf{U}_1 = \tilde{\mathbf{U}}_1 = \cos\left(\frac{\pi}{4}\right)\mathbf{e}_1 + \sin\left(\frac{\pi}{4}\right)\mathbf{e}_2, \mathbf{U}_2 = \mathbf{e}_2, \tilde{\mathbf{U}}_2 = \cos\left(\frac{4\pi}{6}\right)\mathbf{e}_1 + \sin\left(\frac{4\pi}{6}\right)\mathbf{e}_2$	$= 0$	$= 0$

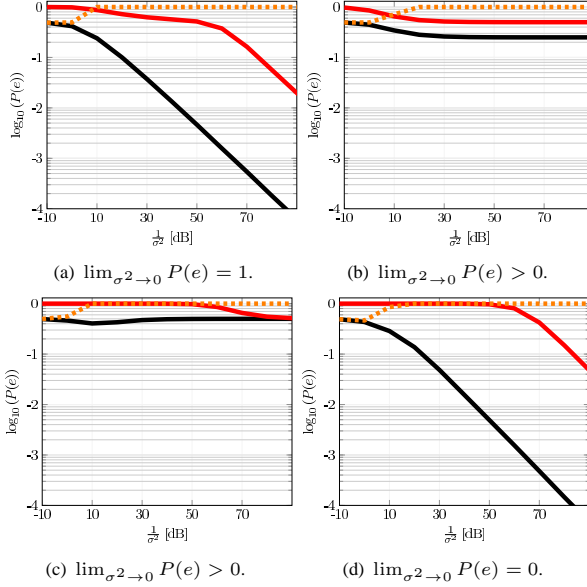


Fig. 3. Simulation results for the examples in Table 1. In all plots black line corresponds to true error probability $P(e)$, red line corresponds to the proposed upper bound to error probability $\bar{P}(e)$ and dashed orange line corresponds to the upper bound proposed in [26].

Fig. 3 shows the simulation results corresponding to each example. Note that the proposed upper bound to the error probability and the derived sufficient conditions give a sharp predictions of an error floor, and also that the bound proposed by [26] always exhibits an error floor.

In example (a), conditions (16) and (17) are satisfied and $d > 0$. Therefore, via Theorem 2, the upper bound to the error probability approaches zero, which also implies that the true error probability approaches zero, in the low-noise regime. In example (b), condition (16) in Theorem 2 is not satisfied for $(i, j) = (1, 2)$, i.e. $\text{im}(\mathbf{W}_{12}) = \text{im}(\mathbf{e}_2) \not\subseteq \text{ker}(\tilde{\mathbf{U}}'_{21}) = \text{im}(\mathbf{e}_1)$, therefore, via Theorem 2 we conclude that the upper bound exhibits an error floor. The results in Fig. 3 show that in this case the true error probability also exhibits an error floor.

For examples (c) and (d) the intuition is provided by the Corollary 2, where in the case of the one-dimensional subspaces the concept of principal angles simply reduces to the notion of angle between two lines. In particular, in example (c) the condition (27) in Corollary 2 is not satisfied for $(i, j) = (1, 2)$, and we observe an error floor in the true error probability. On the contrary, in example (d) the conditions (27) in Corollary 2 are satisfied which immediately implies perfect classification in the low-noise regime.

Consider now the following 2-class example in \mathbb{R}^6 with orthonormal basis vectors $\mathbf{e}_i, i = 1, \dots, 6$, where the signal

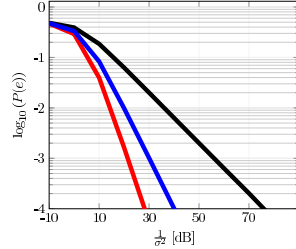


Fig. 4. Black, blue and red line correspond to the true error probabilities for examples given in (35), (36) and (37), respectively.

subspaces are:

$$\mathbf{U}_1 = [\mathbf{e}_1, \mathbf{e}_2, \mathbf{e}_3], \quad \mathbf{U}_2 = [\mathbf{e}_4, \mathbf{e}_5, \mathbf{e}_6] \quad (34)$$

and various mismatched subspaces are:

$$\tilde{\mathbf{U}}_1 = [\mathbf{e}_1], \quad \tilde{\mathbf{U}}_2 = [\mathbf{e}_4] \quad (35)$$

$$\tilde{\mathbf{U}}_1 = [\mathbf{e}_1, \mathbf{e}_2], \quad \tilde{\mathbf{U}}_2 = [\mathbf{e}_4, \mathbf{e}_5] \quad (36)$$

$$\tilde{\mathbf{U}}_1 = \mathbf{U}_1, \quad \tilde{\mathbf{U}}_2 = \mathbf{U}_2. \quad (37)$$

It is straightforward to verify that the sufficient conditions for perfect classification given by Theorem 2 hold for all three pairs of mismatch models (35), (36) and (37). Furthermore, one can also determine the values of d as 0.5, 1 and 1.5, where values of d do not depend on α_{ij} , for the mismatched models given by (35), (36) and (37), respectively. As observed in Section III a higher value of d implies a higher robustness to noise. Simulation results of the true error probability are given in Fig. 4, where one can observe that increasing values of d (associated with the upper bound to the error probability) correspond to steeper decrease of the true error probability as $\sigma^2 \rightarrow 0$.

V. APPLICATION: MOTION SEGMENTATION

We finally show how theory can also capture the impact of mismatch on classification performance in an application involving real world data. We consider a motion segmentation application, where the goal is to segment a video in multiple rigidly moving objects. The problem is usually solved by extracting feature points from the video and tracking their position over different frames. In more details, in this application, observation vectors \mathbf{y} are obtained by stacking the coordinate values associated to a given feature point corresponding to different frames, and the objective of motion segmentation is that of classifying each feature point as belonging to one of the moving objects in the video [10].

We concentrate on a semi supervised learning approach, in which only few vectors corresponding to features points are manually labeled, whereas the remaining points are classified automatically. In this sense, points that are manually labeled

can be interpreted as labeled training samples. Our aim is to determine the minimum number of training samples needed to guarantee reliable classification of the remaining features points.

We use the Hopkins 155 motion segmentation dataset [31], which consists of video sequences with 2 or 3 motions in each video. In particular, we consider a video with 3 motions⁹, where number of samples of class 1, class 2 and class 3 is 236, 142 and 114, respectively. The rule adopted to pick the video was the maximal possible feature points – samples – for each motion. We will refer to different motions as classes.

The “true model” in this case is obtained by supervised training over all data samples. The class-conditioned covariance matrices are obtained by retaining only the first 4 principal components of the estimated covariances obtained via the maximum likelihood (ML) estimator¹⁰ for each class. The number of principal components retained is justified theoretically [10], [11], [12] and also empirically by observing the fast decay of the covariance matrix eigenvalues. In fact, features points trajectories belonging to a given motion can be shown to lie on approximately 3 dimensional affine spaces or 4 dimensional linear spaces (see [10] for additional information about the datasets).

Experimental results are produced as follows: first, the dataset samples are split randomly into a training set and a testing set, where the training set contains n_{\max} samples per class and the remaining samples of each class are used to form the test set. Then, n_1 , n_2 and n_3 samples are drawn from the training set corresponding to class 1, class 2 and class 3, respectively. For each class, the signal covariance is obtained via the ML estimator and by retaining only the first 4 principal components, in the same way as for the “true model”. The error rate of the MMAP classifier is then evaluated on the testing set for numbers of training samples n_1 , n_2 and n_3 ranging from 4 to $n_{\max} = 90$. At the same time, we also determine if sufficient conditions for perfect classification as in Theorem 2 hold. We run 1000 experiments where in each run the data is split randomly into training and testing set.

The particular choice of samples in the training set can lead to high variability in the mismatched models, especially for small number of training samples. Therefore, in the following, we have chosen to report the results as follows:

- we state that analysis predicts reliable classification if the sufficient conditions in Theorem 2 hold with probability p_p over the different experiment runs;
- we also state that simulation predicts reliable classification if the true error probability is 0 with probability p_p over different experiment runs.

The results for probabilities $p_p = 0.8$, $p_p = 0.9$ and $n_3 = 70$ are reported in Fig. 5.

We observe that the phase transition predicted by analysis approximates reasonably well the phase transition obeyed by simulation. In particular, we can use our theory to gauge the number of training samples required for perfect classification in the low-noise regime. As expected, we also observe that

⁹Denoted as “1RT2RCR” in the dataset.

¹⁰Note that this is equivalent to computing the empirical covariance matrix.

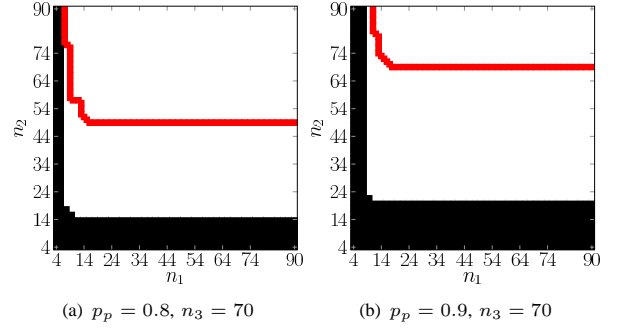


Fig. 5. Phase transition of true error rate and phase transition given by the upper bound to the error probability as a function of number of training samples n_1 , n_2 . Black corresponds to an error floor of the true error rate, white corresponds to reliable classification, and red line denotes the phase transition predicted via Theorem 2 for a given probability p_p .

the larger value of p_p gives more conservative estimates of the required training samples. This holds for both simulation and analysis.

We also observe that identical trends hold for other values of n_3 . In particular, for $n_3 < 30$ simulation does not show a phase transition and likewise analysis does not show a phase transition either (these experiments are not reported in view of space limitations). In contrast, for $n_3 \geq 30$ both simulation and analysis predict a phase transition in the error probability.

Finally, note that real data are not drawn from Gaussian distributions or perfect linear subspaces (the two main ingredients underlying our analysis). Nevertheless, we have shown that the derived bound has a practical value even when the two assumption do not hold strictly.

VI. CONCLUSION

This paper studies the classification of linear subspaces with mismatched classifiers, i.e. classifiers that operate on a mismatched version of the signal parameters *in lieu* of the true signal parameters. In particular, we have developed a low-noise expansion of an upper bound to the error probability of such a mismatched classifier that equips one with a set of sufficient conditions – which are a function of the geometry of the true signal distributions, the geometry of the mismatched signal distributions, and their interplay – in order to understand whether it is possible to classify reliably in the presence of mismatch in the low-noise regime.

Such sufficient conditions are shown to be sharp in the sense that they can predict the presence (and the absence) of a classification error floor both in experiments involving synthetic data as well as experiments involving real data. These conditions have also been shown to gauge well the number of training samples required for reliable classification in a semi-supervised motion segmentation application using the Hopkins 155 data set.

Overall, we argue that our conditions can also be used as a proxy to develop linear feature extraction methods that are robust to mismatch. In particular, our study suggests that such methods ought to orthogonalize the different classes as much as possible in order to tolerate model mismatch. This intuition has been pursued in recent state-of-the-art linear feature extraction methods.

APPENDIX

A. Preliminaries

We introduce additional quantities that are useful for the proofs of Theorems 1 and 2 and other results. We define the projection operators:

$$\mathbf{P}_i = \mathbf{U}_i \mathbf{U}_i^T \quad (38)$$

$$\tilde{\mathbf{P}}_i = \tilde{\mathbf{U}}_i \tilde{\mathbf{U}}_i^T \quad (39)$$

$$\tilde{\mathbf{P}}'_{ij} = \tilde{\mathbf{U}}'_{ij} (\tilde{\mathbf{U}}'_{ij})^T \quad (40)$$

where \mathbf{U}_i , $\tilde{\mathbf{U}}_i$ and $\tilde{\mathbf{U}}'_{ij}$ are given as in Section II-A. In addition to the bases \mathbf{U}_i and $\tilde{\mathbf{U}}_i$ for the $\text{im}(\Sigma_i)$ and $\text{im}(\tilde{\Sigma}_i)$, respectively, we also introduce the bases for the $\ker(\Sigma_i)$ and $\ker(\tilde{\Sigma}_i)$ as $\mathbf{U}_i^\perp \in \mathbb{R}^{N \times N-r_i}$ and $\tilde{\mathbf{U}}_i^\perp \in \mathbb{R}^{N \times N-\tilde{r}_i}$, respectively. We define the projection operators onto these subspaces:

$$\mathbf{K}_i = \mathbf{U}_i^\perp (\mathbf{U}_i^\perp)^T \quad (41)$$

$$\tilde{\mathbf{K}}_i = \tilde{\mathbf{U}}_i^\perp (\tilde{\mathbf{U}}_i^\perp)^T. \quad (42)$$

Finally, we define

$$\mathbf{L}_i = \mathbf{U}_i (\text{diag}(\lambda_1^i, \dots, \lambda_{r_i}^i) + \sigma^2 \mathbf{I})^{-1} (\mathbf{U}_i)^T \quad (43)$$

$$\tilde{\mathbf{L}}_i = \tilde{\mathbf{U}}_i (\text{diag}(\tilde{\lambda}_1^i, \dots, \tilde{\lambda}_{\tilde{r}_i}^i) + \sigma^2 \mathbf{I})^{-1} (\tilde{\mathbf{U}}_i)^T. \quad (44)$$

We also write

$$\Sigma_{ij} = \mathbf{L}_{ij} + \frac{1}{\sigma^2} \mathbf{K}_{ij}, \quad (45)$$

where $\mathbf{L}_{ij} = \mathbf{L}_i + \alpha_{ij} \tilde{\mathbf{L}}_j - \alpha_{ij} \tilde{\mathbf{L}}_i$ and $\mathbf{K}_{ij} = \mathbf{K}_i + \alpha_{ij} \tilde{\mathbf{K}}_j - \alpha_{ij} \tilde{\mathbf{K}}_i$. Note that

$$\mathbf{K}_{ij} = \mathbf{K}_i + \alpha_{ij} \tilde{\mathbf{P}}_i - \alpha_{ij} \tilde{\mathbf{P}}_j \quad (46)$$

$$= \mathbf{K}_i + \alpha_{ij} \tilde{\mathbf{P}}'_{ij} - \alpha_{ij} \tilde{\mathbf{P}}'_{ji} \quad (47)$$

in view of the fact that $\mathbf{P}_i + \mathbf{K}_i = \mathbf{I}$ and $\tilde{\mathbf{P}}_i + \tilde{\mathbf{K}}_i = \mathbf{I}$ and $\tilde{\mathbf{P}}_i - \tilde{\mathbf{P}}_j = \tilde{\mathbf{P}}'_{ij} - \tilde{\mathbf{P}}'_{ji}$. The last equality simply follows from the definition of $\tilde{\mathbf{P}}'_{ij}$ and $\tilde{\mathbf{P}}'_{ji}$, and the definitions of $\tilde{\mathbf{U}}'_{ij}$, $\tilde{\mathbf{U}}'_{ji}$ and $\tilde{\mathbf{U}}_{ij}^\cap$ given in Section II-A:

$$\begin{aligned} \tilde{\mathbf{P}}_i - \tilde{\mathbf{P}}_j &= \tilde{\mathbf{U}}'_{ij} (\tilde{\mathbf{U}}'_{ij})^T + \tilde{\mathbf{U}}_{ij}^\cap (\tilde{\mathbf{U}}_{ij}^\cap)^T \\ &\quad - \left(\tilde{\mathbf{U}}'_{ji} (\tilde{\mathbf{U}}'_{ji})^T + \tilde{\mathbf{U}}_{ij}^\cap (\tilde{\mathbf{U}}_{ij}^\cap)^T \right) \end{aligned} \quad (48)$$

$$= \tilde{\mathbf{P}}'_{ij} - \tilde{\mathbf{P}}'_{ji}. \quad (49)$$

We also introduce results that are useful for the proof of the main Theorems. We first show that

$$\ker((\tilde{\mathbf{U}}'_{ij})^T) = \ker(\tilde{\mathbf{P}}'_{ij}) = \ker(\tilde{\mathbf{U}}_i) + (\text{im}(\tilde{\mathbf{U}}_i) \cap \text{im}(\tilde{\mathbf{U}}_j)). \quad (50)$$

By leveraging the definition of $\tilde{\mathbf{P}}'_{ij}$ in (40) we have

$$\ker(\tilde{\mathbf{P}}'_{ij}) = (\text{im}(\tilde{\mathbf{P}}'_{ij}))^\perp = (\text{im}(\tilde{\mathbf{U}}'_{ij}))^\perp = \text{im}([\tilde{\mathbf{U}}'_{ij}, \tilde{\mathbf{U}}_i^\perp]) \quad (51)$$

$$= \ker(\tilde{\mathbf{U}}_i) + (\text{im}(\tilde{\mathbf{U}}_i) \cap \text{im}(\tilde{\mathbf{U}}_j)). \quad (52)$$

We also show that (24) implies the condition (23). In particular, we note that

$\mathbf{V}_{ij}^T (\tilde{\mathbf{U}}'_{ij} (\tilde{\mathbf{U}}'_{ij})^T - \tilde{\mathbf{U}}'_{ji} (\tilde{\mathbf{U}}'_{ji})^T) \mathbf{V}_{ij} = (\mathbf{V}_{ij})^T (\tilde{\mathbf{P}}'_{ij} - \tilde{\mathbf{P}}'_{ji}) \mathbf{V}_{ij}$ and write the following

$$(\mathbf{V}_{ij})^T \tilde{\mathbf{P}}'_{ij} \mathbf{V}_{ij} = (\mathbf{V}_{ij})^T \tilde{\mathbf{U}}'_{ij} (\tilde{\mathbf{U}}'_{ij})^T \mathbf{V}_{ij} \quad (53)$$

$$(\mathbf{V}_{ij})^T \tilde{\mathbf{P}}'_{ji} \mathbf{V}_{ij} = (\mathbf{V}_{ij})^T \tilde{\mathbf{U}}'_{ji} (\tilde{\mathbf{U}}'_{ji})^T \mathbf{V}_{ij}. \quad (54)$$

Note that the singular values of $(\mathbf{V}_{ij})^T \tilde{\mathbf{U}}'_{ij}$ and $(\mathbf{V}_{ij})^T \tilde{\mathbf{U}}'_{ji}$ correspond to the cosines of the principal angles between $\text{im}(\mathbf{V}_{ij})$ and $\text{im}(\tilde{\mathbf{U}}'_{ij})$, and $\text{im}(\mathbf{V}_{ij})$ and $\text{im}(\tilde{\mathbf{U}}'_{ji})$, respectively. We then consider the SVDs

$$(\mathbf{V}_{ij})^T \tilde{\mathbf{U}}'_{ij} = \mathbf{H}_{ij} \mathbf{D}_{ij} \mathbf{J}_{ij}^T \quad (55)$$

$$(\mathbf{V}_{ij})^T \tilde{\mathbf{U}}'_{ji} = \mathbf{H}_{ji} \mathbf{D}_{ji} \mathbf{J}_{ji}^T \quad (56)$$

where the dimensions of matrices \mathbf{H}_{ij} , \mathbf{H}_{ji} , \mathbf{D}_{ij} , \mathbf{D}_{ji} , \mathbf{J}_{ij} and \mathbf{J}_{ji} follow from the dimension of the \mathbf{V}_{ij} , $\tilde{\mathbf{U}}'_{ij}$ and $\tilde{\mathbf{U}}'_{ji}$ as shown in (9). Then, we can express (23) as

$$\mathbf{H}_{ij} \mathbf{D}_{ij} \mathbf{D}_{ij}^T \mathbf{H}_{ij}^T \succ \mathbf{H}_{ji} \mathbf{D}_{ji} \mathbf{D}_{ji}^T \mathbf{H}_{ji}^T. \quad (57)$$

Finally, it is straightforward to see that (24) implies (23).

B. Proof of Theorem 1

We prove Theorem 1 by using the fact that $u(x) \leq \exp(\alpha x)$, $\forall x, \alpha > 0$ and by leveraging the union bound.

Recall from (7) that the error probability associated with the MMAP classifier can be expressed as

$$P(e) = \sum_{i=1}^C p_i \cdot P(e|c=i) \quad (58)$$

where $P(e|c=i) = P(\hat{c} \neq i|c=i)$ is the error probability for signals in class i . Via the union bound, we can state that

$$P(e|c=i) = P(\hat{c} \neq i|c=i) \leq \sum_{j=1, j \neq i}^C P(\hat{c} = j|c=i) \quad (59)$$

where

$$P(\hat{c} = j|c=i) = \int_{-\infty}^{\infty} p(\mathbf{y}|c=i) \quad (60)$$

$$\cdot u\left(\log\left(\frac{\tilde{p}_j \tilde{p}(\mathbf{y}|c=j)}{\tilde{p}_i \tilde{p}(\mathbf{y}|c=i)}\right)\right) d\mathbf{y}. \quad (61)$$

We will denote $P(\hat{c} = j|c=i) = P(e_{ij})$. Now, by letting $\alpha_{ij} > 0 \forall i \neq j$ we can upper bound the step function to obtain

$$\begin{aligned} P(e_{ij}) &\leq \int_{-\infty}^{\infty} p(\mathbf{y}|c=1) \\ &\quad \cdot \exp\left(\alpha_{ij} \log\left(\frac{\tilde{p}_j \tilde{p}(\mathbf{y}|c=j)}{\tilde{p}_i \tilde{p}(\mathbf{y}|c=i)}\right)\right) d\mathbf{y} \\ &= \left(\frac{\tilde{p}_j}{\tilde{p}_i}\right)^{\alpha_{ij}} \left(\frac{|\tilde{\Sigma}_i + \sigma^2 \mathbf{I}|}{|\tilde{\Sigma}_j + \sigma^2 \mathbf{I}|}\right)^{\frac{\alpha_{ij}}{2}} \\ &\quad \cdot ((2\pi)^N |\tilde{\Sigma}_i + \sigma^2 \mathbf{I}|)^{-\frac{1}{2}} \\ &\quad \cdot \int_{-\infty}^{\infty} \exp\left(-\frac{1}{2} \mathbf{y}^T \Sigma_{ij} \mathbf{y}\right) d\mathbf{y} = \bar{P}(e_{ij}), \end{aligned} \quad (62)$$

where we recall

$$\Sigma_{ij} = (\Sigma_i + \sigma^2 \mathbf{I})^{-1} + \alpha_{ij}(\tilde{\Sigma}_j + \sigma^2 \mathbf{I})^{-1} - \alpha_{ij}(\tilde{\Sigma}_i + \sigma^2 \mathbf{I})^{-1}.$$

If $\Sigma_{ij} \succ \mathbf{0} \forall i \neq j$, then the integral in (62) converges $\forall i \neq j$. Therefore, we can bound the error probability as follows:

$$P(e) \leq \bar{P}(e) = \sum_{i=1}^C p_i \cdot \left(\sum_{j=1, j \neq i}^C \bar{P}(e_{ij}) \right) \quad (63)$$

where

$$\bar{P}(e_{ij}) = \left(\frac{\tilde{p}_j}{\tilde{p}_i} \sqrt{\frac{|\tilde{\Sigma}_i + \sigma^2 \mathbf{I}|}{|\tilde{\Sigma}_j + \sigma^2 \mathbf{I}|}} \right)^{\alpha_{ij}} \cdot (|\Sigma_i + \sigma^2 \mathbf{I}| |\Sigma_{ij}|)^{-\frac{1}{2}}. \quad (64)$$

If $\exists i \neq j : \Sigma_{ij} \not\succ \mathbf{0}$ then the integral in (62) does not converge. Therefore, we trivially bound the error probability as $P(e) \leq \bar{P}(e) \leq 1$.

C. Proof of Theorem 2

We prove Theorem 2 in two parts. First, we establish sufficient conditions for $\Sigma_{ij} \succ \mathbf{0}$ and we also establish necessary conditions for $\Sigma_{ij} \succ \mathbf{0}$; second, we establish conditions for the upper bound to the probability of misclassification to approach zero as the noise approaches zero.

1) *Part 1: Positive Definiteness of Σ_{ij} :* Let us consider sufficient conditions for $\Sigma_{ij} \succ \mathbf{0}$. We write

$$\mathbf{x} = \mathbf{x}_{\parallel} + \mathbf{x}_{\perp} = \mathbf{x}_{\mathbf{V}} + \mathbf{x}_{\mathbf{W}} + \mathbf{x}_{\perp}, \quad (65)$$

where

$$\mathbf{x}_{\parallel} = \mathbf{U}_i \mathbf{z}_{\parallel} \quad (66)$$

$$\mathbf{x}_{\perp} = \mathbf{U}_i^{\perp} \mathbf{z}_{\perp} \quad (67)$$

$$\mathbf{x}_{\mathbf{V}} = \mathbf{V}_{ij} \mathbf{z}_{\mathbf{V}} \quad (68)$$

$$\mathbf{x}_{\mathbf{W}} = \mathbf{W}_{ij} \mathbf{z}_{\mathbf{W}}, \quad (69)$$

for some vectors $\mathbf{z}_{\parallel} \in \mathbb{R}^{r_i}$, $\mathbf{z}_{\perp} \in \mathbb{R}^{N-r_i}$, $\mathbf{z}_{\mathbf{V}} \in \mathbb{R}^{s_{ij}^V}$ and $\mathbf{z}_{\mathbf{W}} \in \mathbb{R}^{s_{ij}^W}$. Note also that $\|\mathbf{x}_{\mathbf{V}}\| = \|\mathbf{z}_{\mathbf{V}}\|$, $\|\mathbf{x}_{\mathbf{W}}\| = \|\mathbf{z}_{\mathbf{W}}\|$ and $\|\mathbf{x}_{\perp}\| = \|\mathbf{z}_{\perp}\|$.

Let us first assume that

$$\text{im}(\mathbf{W}_{ij}) \subseteq \ker((\tilde{\mathbf{U}}'_{ji})^T) \quad (70)$$

and that $s_{ij}^V > 0$ and

$$\mathbf{V}_{ij}^T (\tilde{\mathbf{U}}'_{ij} (\tilde{\mathbf{U}}'_{ij})^T - \tilde{\mathbf{U}}'_{ji} (\tilde{\mathbf{U}}'_{ji})^T) \mathbf{V}_{ij} \succ \mathbf{0}, \quad (71)$$

$$\alpha_{ij} < \min\left(\frac{\tilde{\lambda}_{\tilde{r}_i}^i}{\lambda_1^i + 1}, \frac{c_0}{1 + c_0(1 + \frac{1}{\lambda_{\tilde{r}_i}^i})}, 1\right), \quad (72)$$

where $\frac{c_0}{\lambda_1^i + 1}$ is the smallest eigenvalue of $\mathbf{V}_{ij}^T (\tilde{\mathbf{U}}'_{ij} (\tilde{\mathbf{U}}'_{ij})^T - \tilde{\mathbf{U}}'_{ji} (\tilde{\mathbf{U}}'_{ji})^T) \mathbf{V}_{ij} = (\mathbf{V}_{ij})^T (\tilde{\mathbf{P}}'_i - \tilde{\mathbf{P}}'_j) \mathbf{V}_{ij}$. We can easily produce the lower bound

$$\mathbf{x}^T \Sigma_{ij} \mathbf{x} = \mathbf{x}^T \mathbf{L}_{ij} \mathbf{x} + \frac{1}{\sigma^2} \mathbf{x}^T \mathbf{K}_{ij} \mathbf{x} \quad (73)$$

$$= \mathbf{x}^T \mathbf{L}_i \mathbf{x} + \alpha_{ij} \mathbf{x}^T (\tilde{\mathbf{L}}_j - \tilde{\mathbf{L}}_i) \mathbf{x} \quad (74)$$

$$+ \frac{1}{\sigma^2} (\mathbf{x}^T \mathbf{K}_i \mathbf{x} + \alpha_{ij} \mathbf{x}^T (\tilde{\mathbf{K}}_j - \tilde{\mathbf{K}}_i) \mathbf{x}) \quad (74)$$

$$\geq \mathbf{c}^T \mathbf{C} \mathbf{c}, \quad (75)$$

where $\mathbf{c} = [\|\mathbf{x}_{\mathbf{W}}\|, \|\mathbf{x}_{\mathbf{V}}\|, \|\mathbf{x}_{\perp}\|]^T$ and

$$\mathbf{C} = \begin{bmatrix} \frac{1}{\lambda_1^i + 1} - \frac{\alpha_{ij}}{\tilde{\lambda}_{\tilde{r}_i}^i} & 0 & 0 \\ 0 & \frac{1}{\lambda_1^i + 1} - \frac{\alpha_{ij}}{\tilde{\lambda}_{\tilde{r}_i}^i} + \frac{c_0 \alpha_{ij}}{\sigma^2} & -\frac{\alpha_{ij}}{\sigma^2} \\ 0 & -\frac{\alpha_{ij}}{\sigma^2} & \frac{1 - \alpha_{ij}}{\sigma^2} - \frac{\alpha_{ij}}{\tilde{\lambda}_{\tilde{r}_i}^i} \end{bmatrix}, \quad (76)$$

by using the equalities and inequalities

$$\mathbf{x}^T \mathbf{L}_i \mathbf{x} \geq \frac{1}{\lambda_1^i + 1} \|\mathbf{x}_{\parallel}\|^2 \quad (77)$$

$$\mathbf{x}^T (\tilde{\mathbf{L}}_j - \tilde{\mathbf{L}}_i) \mathbf{x} \geq -\frac{1}{\tilde{\lambda}_{\tilde{r}_i}^i} \|\mathbf{x}\|^2 \quad (78)$$

$$\mathbf{x}^T \mathbf{K}_i \mathbf{x} = \|\mathbf{x}_{\perp}\|^2 \quad (79)$$

$$\mathbf{x}^T (\tilde{\mathbf{K}}_j - \tilde{\mathbf{K}}_i) \mathbf{x} \geq c_0 \|\mathbf{x}_{\mathbf{V}}\|^2 - 2 \|\mathbf{x}_{\mathbf{V}}\| \|\mathbf{x}_{\perp}\| - \|\mathbf{x}_{\perp}\|^2. \quad (80)$$

The inequality in (77) is due to the fact that $\mathbf{x}_{\parallel} \in \text{im}(\mathbf{L}_i) = \text{im}(\mathbf{U}_i)$ and $\frac{1}{\lambda_1^i + 1}$ is a lower bound to the minimum positive eigenvalue of $\tilde{\mathbf{L}}_i$. The inequality in (78) is due to the fact that $\tilde{\mathbf{L}}_j$ is positive semidefinite and that $\frac{1}{\tilde{\lambda}_{\tilde{r}_i}^i}$ is an upper bound for the largest eigenvalue of $\tilde{\mathbf{L}}_i$. The inequality in (79) follows from the definition of the projector \mathbf{K}_i . Finally, the inequality in (80) can be obtained by noting that (69) implies $\mathbf{x}_{\mathbf{W}} \in \text{im}(\mathbf{W}_{ij}) = \text{im}(\Sigma_i) \cap \ker(\tilde{\mathbf{P}}'_{ij})$, and the condition (70) also implies $\mathbf{x}_{\mathbf{W}} \in \ker(\tilde{\mathbf{P}}'_{ji}) = \ker((\tilde{\mathbf{U}}'_{ji})^T)$. Then, we can write

$$\mathbf{x}^T (\tilde{\mathbf{K}}_j - \tilde{\mathbf{K}}_i) \mathbf{x} = \mathbf{x}^T (\tilde{\mathbf{P}}'_{ij} - \tilde{\mathbf{P}}'_{ji}) \mathbf{x} \quad (81)$$

$$= \mathbf{x}_{\mathbf{V}}^T (\tilde{\mathbf{P}}'_{ij} - \tilde{\mathbf{P}}'_{ji}) \mathbf{x}_{\mathbf{V}} + 2 \mathbf{x}_{\mathbf{V}}^T (\tilde{\mathbf{P}}'_{ij} - \tilde{\mathbf{P}}'_{ji}) \mathbf{x}_{\perp} + \mathbf{x}_{\perp}^T (\tilde{\mathbf{P}}'_{ij} - \tilde{\mathbf{P}}'_{ji}) \mathbf{x}_{\perp} \quad (82)$$

and we note that condition (71) implies the lower bound $\mathbf{x}_{\mathbf{V}}^T (\tilde{\mathbf{P}}'_{ij} - \tilde{\mathbf{P}}'_{ji}) \mathbf{x}_{\mathbf{V}} \geq c_0 \|\mathbf{x}_{\mathbf{V}}\|^2$. Moreover, all the eigenvalues of $\tilde{\mathbf{P}}'_{ij} - \tilde{\mathbf{P}}'_{ji}$ are contained in the interval $[-1, 1]$ [32, Theorem 26], so that $\mathbf{x}_{\perp}^T (\tilde{\mathbf{P}}'_{ij} - \tilde{\mathbf{P}}'_{ji}) \mathbf{x}_{\perp} \geq -\|\mathbf{x}_{\perp}\|^2$, and, on leveraging Cauchy-Schwarz inequality, we also have $\mathbf{x}_{\mathbf{V}}^T (\tilde{\mathbf{P}}'_{ij} - \tilde{\mathbf{P}}'_{ji}) \mathbf{x}_{\perp} \geq -2 \|\mathbf{x}_{\mathbf{V}}\| \|\mathbf{x}_{\perp}\|$. Now, by using standard algebraic manipulations, it is possible to show that the choice (72) leads to $\mathbf{C} \succ \mathbf{0}$, hence $\Sigma_{ij} \succ \mathbf{0}$, $\forall \sigma^2 \in (0, \min(1, \frac{1 - \alpha_{ij}}{\alpha_{ij}} \tilde{\lambda}_{\tilde{r}_i}^i))$.

Let us now assume that

$$\text{im}(\mathbf{W}_{ij}) \subseteq \ker((\tilde{\mathbf{U}}'_{ji})^T) \quad (83)$$

and that $s_{ij}^V = 0$ and

$$\alpha_{ij} < \min\left(\frac{\tilde{\lambda}_{\tilde{r}_i}^i}{\lambda_1^i + 1}, \frac{\tilde{\lambda}_{\tilde{r}_i}^i}{\tilde{\lambda}_{\tilde{r}_i}^i + 1}, 1\right). \quad (84)$$

We can now produce the lower bound

$$\mathbf{x}^T \Sigma_{ij} \mathbf{x} \geq \frac{1}{\lambda_1^i + 1} \|\mathbf{x}_{\parallel}\|^2 - \frac{\alpha_{ij}}{\tilde{\lambda}_{\tilde{r}_i}^i} \|\mathbf{x}\|^2 + \frac{1}{\sigma^2} \left(\|\mathbf{x}_{\perp}\|^2 + \alpha_{ij} \mathbf{x}^T (\tilde{\mathbf{P}}'_{ij} - \tilde{\mathbf{P}}'_{ji}) \mathbf{x} \right) \quad (85)$$

$$\geq \left(\frac{1}{\lambda_1^i + 1} - \frac{\alpha_{ij}}{\tilde{\lambda}_{\tilde{r}_i}^i} \right) \|\mathbf{x}_{\parallel}\|^2 + \left(\frac{1 - \alpha_{ij}}{\sigma^2} - \frac{\alpha_{ij}}{\tilde{\lambda}_{\tilde{r}_i}^i} \right) \|\mathbf{x}_{\perp}\|^2, \quad (86)$$

by using the inequalities in (77)-(80) and by noting that $\mathbf{x}_V = \mathbf{0}$. The choice (84) then leads to $\Sigma_{ij} \succ \mathbf{0}$, $\forall \sigma^2 \in (0, \min(1, \frac{1-\alpha_{ij}}{\alpha_{ij}} \tilde{\lambda}_i^r))$.

We now briefly show that condition (16) is necessary for $\Sigma_{ij} \succ \mathbf{0}$. In particular, if $\text{im}(\mathbf{W}_{ij}) \not\subseteq \ker((\tilde{\mathbf{U}}'_{ji})^T)$, then $\exists \mathbf{x} : \mathbf{x}^T \Sigma_{ij} \mathbf{x} < 0 \forall \sigma^2 < \sigma_*^2$. Pick any $\alpha_{ij} > 0$ and take $\mathbf{x} = \mathbf{x}_W$. We can show that the decomposition in (73) can be bounded as $\mathbf{x}_W^T \mathbf{L}_{ij} \mathbf{x}_W < b_1$, with $b_1 > 0$. Due to the fact that $\mathbf{x}_W \in \text{im}(\mathbf{U}_i)$ we can also write $\mathbf{x}_W^T \mathbf{K}_{ij} \mathbf{x}_W = \mathbf{x}_W^T (\tilde{\mathbf{P}}'_{ij} - \tilde{\mathbf{P}}'_{ji}) \mathbf{x}_W$. Then, because also $\mathbf{x}_W \in \ker((\tilde{\mathbf{U}}'_{ji})^T)$ we can write $\mathbf{x}_W^T \mathbf{K}_{ij} \mathbf{x}_W = -\mathbf{x}_W^T \tilde{\mathbf{P}}'_{ji} \mathbf{x}_W$. Now, since $\text{im}(\mathbf{W}_{ij}) \not\subseteq \ker((\tilde{\mathbf{U}}'_{ji})^T)$, it is clear that $\mathbf{x}_W^T \mathbf{K}_{ij} \mathbf{x}_W < -b_2$, with $b_2 > 0$. Therefore $\mathbf{x}^T \Sigma_{ij} \mathbf{x} < 0$ for all $\sigma^2 < \frac{b_1 \alpha_{ij}}{b_2}$.

By following the same line of reasoning one can also show that if the smallest eigenvalue of $\mathbf{V}_{ij}^T (\tilde{\mathbf{U}}'_{ij} (\tilde{\mathbf{U}}'_{ij})^T - \tilde{\mathbf{U}}'_{ji} (\tilde{\mathbf{U}}'_{ji})^T) \mathbf{V}_{ij}$ is negative $\exists \mathbf{x} \in \text{im}(\mathbf{V}_{ij}) : \mathbf{x}^T \Sigma_{ij} \mathbf{x} < 0 \forall \sigma^2 < \sigma_*^2$. This condition is closely related to (17) where we require the smallest eigenvalue to be greater than 0.

2) *Part 2: Low-noise Expansion:* Let us now consider conditions for the upper bound to the probability of misclassification to approach zero as the noise approaches zero.

Assume that sufficient conditions for positive definiteness of $\Sigma_{ij}, \forall i \neq j$ do not hold. Then, the upper bound to the probability of error is chosen to be $\bar{P}(e) = 1$, so that in general it does not tend to zero as σ^2 tends to zero.

Assume now that the sufficient conditions for $\Sigma_{ij} \succ \mathbf{0}$ as given in Section VI-C1 hold $\forall i \neq j$. Then, the upper bound to the probability of misclassification can be written as follows:

$$\bar{P}(e) = \sum_i \sum_{j \neq i} p_i \left(\frac{\tilde{p}_j}{\tilde{p}_i} \sqrt{\frac{|\tilde{\Sigma}_i + \sigma^2 \mathbf{I}|}{|\tilde{\Sigma}_j + \sigma^2 \mathbf{I}|}} \right)^{\alpha_{ij}} \cdot (|\Sigma_i + \sigma^2 \mathbf{I}| |\Sigma_{ij}|)^{-\frac{1}{2}}. \quad (87)$$

We will now produce a low-noise expansion of (87) in order to understand whether or not $\lim_{\sigma^2 \rightarrow 0} \bar{P}(e) = 0$. The following low-noise expansions are trivial:

$$|\Sigma_i + \sigma^2 \mathbf{I}| = \left(\prod_{k=1}^{r_i} (\lambda_k^i + \sigma^2) \right) (\sigma^2)^{N-r_i} \quad (88)$$

$$= \mathcal{O}((\sigma^2)^{N-r_i}), \quad \sigma^2 \rightarrow 0 \quad (89)$$

$$|\tilde{\Sigma}_i + \sigma^2 \mathbf{I}| = \left(\prod_{k=1}^{\tilde{r}_i} (\tilde{\lambda}_k^i + \sigma^2) \right) (\sigma^2)^{N-\tilde{r}_i} \quad (90)$$

$$= \mathcal{O}((\sigma^2)^{N-\tilde{r}_i}), \quad \sigma^2 \rightarrow 0. \quad (91)$$

The low-noise expansion

$$|\Sigma_{ij}| = |\mathbf{L}_{ij} + \frac{1}{\sigma^2} \mathbf{K}_{ij}| \quad (92)$$

is more involved.

Consider the eigenvalue decomposition of \mathbf{K}_{ij} :

$$\mathbf{K}_{ij} = \mathbf{U}_{\mathbf{K}_{ij}} \begin{bmatrix} \Lambda_{\mathbf{K}_{ij}} & \mathbf{0} \\ \mathbf{0} & \mathbf{0} \end{bmatrix} \mathbf{U}_{\mathbf{K}_{ij}}^T, \quad (93)$$

where $\mathbf{U}_{\mathbf{K}_{ij}}$ is orthogonal and $\Lambda_{\mathbf{K}_{ij}} = \text{diag}(\lambda_1^{\mathbf{K}_{ij}}, \dots, \lambda_{r_{\mathbf{K}_{ij}}}^{\mathbf{K}_{ij}})$ contains the positive eigenvalues of \mathbf{K}_{ij} , with $r_{\mathbf{K}_{ij}} =$

$\text{rank}(\mathbf{K}_{ij})$. First, we show that the sufficient conditions (71), (72) or (84) imply that $\mathbf{K}_{ij} \succeq \mathbf{0}$ and $\text{rank}(\mathbf{K}_{ij}) = N + s_{ij}^V - r_i$. We consider separately the cases when $s_{ij}^V > 0$ and $s_{ij}^V = 0$.

Assume $s_{ij}^V > 0$ and that condition in (71) and (72) are satisfied. By definition, $\text{im}(\mathbf{W}_{ij}) = \text{im}(\Sigma_i) \cap \ker(\tilde{\mathbf{P}}'_{ij})$ and, as a consequence of (70), it also holds $\text{im}(\mathbf{W}_{ij}) \subseteq \ker(\tilde{\mathbf{P}}'_{ji})$, which leads to $\text{im}(\mathbf{W}_{ij}) \subseteq \ker(\mathbf{K}_{ij})$. Moreover, it is straightforward to note that $\text{im}([\mathbf{V}_{ij}, \mathbf{U}_i^\perp]) = (\text{im}(\mathbf{W}_{ij}))^\perp$. Then, in order to prove that $\mathbf{K}_{ij} \succeq \mathbf{0}$, we show that $\mathbf{x}^T \Sigma_{ij} \mathbf{x} = \mathbf{x}^T (\mathbf{K}_i + \alpha_{ij} (\tilde{\mathbf{P}}'_{ij} - \tilde{\mathbf{P}}'_{ji})) \mathbf{x} > 0, \forall \mathbf{x} \in \text{im}([\mathbf{V}_{ij}, \mathbf{U}_i^\perp])$. Namely, by leveraging the inequalities in (79) and (80), we can write

$$\begin{aligned} \mathbf{x}^T (\mathbf{K}_i + \alpha_{ij} (\tilde{\mathbf{P}}'_{ij} - \tilde{\mathbf{P}}'_{ji})) \mathbf{x} &\geq (1 - \alpha_{ij}) \|\mathbf{x}_\perp\|^2 \\ &\quad - 2\alpha_{ij} \|\mathbf{x}_\perp\| \|\mathbf{x}_V\| \\ &\quad + \alpha_{ij} c_0 \|\mathbf{x}_V\|^2, \end{aligned} \quad (94)$$

where $\mathbf{x}_\perp, \mathbf{x}_V$ have been defined in (67) and (68). If $\alpha_{ij} < \frac{c_0}{c_0+1}$ then the right hand side of (94) is always strictly positive, unless $\mathbf{x} = \mathbf{0}$. Then, since the condition in (72) implies $\alpha_{ij} < \frac{c_0}{c_0+1}$, we can conclude that $\mathbf{K}_{ij} \succeq \mathbf{0}$ and $\text{im}(\mathbf{W}_{ij}) = \ker(\mathbf{K}_{ij})$ and $\text{im}([\mathbf{V}_{ij}, \mathbf{U}_i^\perp]) = \text{im}(\mathbf{K}_{ij})$. Therefore, $\text{rank}(\mathbf{K}_{ij}) = \text{rank}([\mathbf{V}_{ij}, \mathbf{U}_i^\perp]) = s_{ij}^V + (N - r_i)$.

Assume now $s_{ij}^V = 0$ and that condition in (84) is satisfied. In this case $\mathbf{x}^T \Sigma_{ij} \mathbf{x} = \mathbf{x}^T (\mathbf{K}_i + \alpha_{ij} (\tilde{\mathbf{P}}'_{ij} - \tilde{\mathbf{P}}'_{ji})) \mathbf{x} = \mathbf{x}_\perp^T (\mathbf{K}_i + \alpha_{ij} (\tilde{\mathbf{P}}'_{ij} - \tilde{\mathbf{P}}'_{ji})) \mathbf{x}_\perp \geq \|\mathbf{x}_\perp\|^2 (1 - \alpha_{ij})$, where we have used the fact that eigenvalues of $\tilde{\mathbf{P}}'_{ji} - \tilde{\mathbf{P}}'_{ij}$ contained in the interval $[-1, 1]$. Since (84) implies $\alpha_{ij} < 1$ we conclude, via an argument similar to that in previous paragraph, that $\mathbf{K}_{ij} \succeq \mathbf{0}$ and $\text{rank}(\mathbf{K}_{ij}) = \text{rank}(\mathbf{U}_i^\perp) = s_{ij}^V + (N - r_i)$.

Now, we can write

$$|\mathbf{L}_{ij} + \frac{1}{\sigma^2} \mathbf{K}_{ij}| = \left| \begin{bmatrix} \frac{1}{\sigma^2} \Lambda_{\mathbf{K}_{ij}} & \mathbf{0} \\ \mathbf{0} & \mathbf{0} \end{bmatrix} + \mathbf{E} \right|, \quad (95)$$

where $\mathbf{E} = \mathbf{U}_{\mathbf{K}_{ij}}^T \mathbf{L}_{ij} \mathbf{U}_{\mathbf{K}_{ij}}$. We also denote by $\mathbf{E}_{i_1 \dots i_m}$ the principal submatrix of order $N - m$ obtained by deleting the rows and the columns i_1, \dots, i_m of the matrix \mathbf{E} . Note that $\mathbf{E}_{i_1 \dots i_m} = \mathbf{P}_{i_1 \dots i_m}^T \mathbf{E} \mathbf{P}_{i_1 \dots i_m}$, where the matrix $\mathbf{P}_{i_1 \dots i_m} \in \mathbb{R}^{N \times N-m}$ is obtained by picking all the columns from the identity matrix with the column indices different from i_1, \dots, i_m . Then, the Poincaré separation theorem [33, Corollary 4.3.37] guarantees that the eigenvalues $\mathbf{E}_{i_1 \dots i_m}$ are bounded by the minimum and the maximum eigenvalues of \mathbf{E} , which correspond to the minimum and maximum eigenvalues of \mathbf{L}_{ij} . Moreover, as $\sigma^2 \rightarrow 0$, while the diagonal elements of $\frac{1}{\sigma^2} \Lambda_{\mathbf{K}_{ij}}$ grow unbounded, the eigenvalues of \mathbf{L}_{ij} , and therefore, also the determinant of $\mathbf{E}_{i_1 \dots i_m}$, are bounded.

Then, we can use the determinant decomposition in [34, Theorem 2.3] to express $|\mathbf{L}_{ij} + \frac{1}{\sigma^2} \mathbf{K}_{ij}|$ as follows. If $r_{\mathbf{K}_{ij}} = N$:

$$|\mathbf{L}_{ij} + \frac{1}{\sigma^2} \mathbf{K}_{ij}| = \left| \frac{1}{\sigma^2} \mathbf{K}_{ij} \right| + |\mathbf{L}_{ij}| + S_1 + \dots + S_{N-1}, \quad (96)$$

where

$$S_m = \sum_{1 \leq i_1 < \dots < i_m \leq N} \left(\frac{1}{\sigma^2} \lambda_{i_1}^{\mathbf{K}_{ij}} \right) \dots \left(\frac{1}{\sigma^2} \lambda_{i_m}^{\mathbf{K}_{ij}} \right) |\mathbf{E}_{i_1 \dots i_m}| \quad 1 \leq m \leq N-1 \quad (97)$$

and the summation is over all possible ordered subsets of m indices from the set $\{1, \dots, r_{\mathbf{K}_{ij}}\}$. Otherwise, if $r_{\mathbf{K}_{ij}} < N$:

$$|\mathbf{L}_{ij} + \frac{1}{\sigma^2} \mathbf{K}_{ij}| = |\mathbf{L}_{ij}| + S_1 + \dots + S_{r_{\mathbf{K}_{ij}}}, \quad (98)$$

where

$$S_m = \sum_{1 \leq i_1 < \dots < i_m \leq r_{\mathbf{K}_{ij}}} \left(\frac{1}{\sigma^2} \lambda_{i_1}^{\mathbf{K}_{ij}} \right) \dots \left(\frac{1}{\sigma^2} \lambda_{i_m}^{\mathbf{K}_{ij}} \right) |\mathbf{E}_{i_1 \dots i_m}| \quad 1 \leq m \leq r_{\mathbf{K}_{ij}}. \quad (99)$$

Now, as $\sigma^2 \rightarrow 0$ we can write

$$|\mathbf{L}_{ij} + \frac{1}{\sigma^2} \mathbf{K}_{ij}| = v_{ij} \cdot \left(\frac{1}{\sigma^2} \right)^{r_{\mathbf{K}_{ij}}} + \mathcal{O} \left(\left(\frac{1}{\sigma^2} \right)^{r_{\mathbf{K}_{ij}}-1} \right), \quad (100)$$

where v_{ij} is given by

$$v_{ij} = \begin{cases} \text{pdet}(\mathbf{K}_{ij}) |(\mathbf{U}_{\mathbf{K}_{ij}}^\perp)^T \mathbf{L}_{ij}^0 \mathbf{U}_{\mathbf{K}_{ij}}^\perp| & \text{if } \text{rank}(\mathbf{K}_{ij}) < N \\ |\mathbf{K}_{ij}| & \text{if } \text{rank}(\mathbf{K}_{ij}) = N \end{cases} \quad (101)$$

where $\mathbf{L}_{ij}^0 = \lim_{\sigma^2 \rightarrow 0} \mathbf{L}_{ij} = \mathbf{L}_i^0 + \alpha_{ij} \tilde{\mathbf{L}}_j^0 - \alpha_{ij} \tilde{\mathbf{L}}_i^0$ and

$$\mathbf{L}_i^0 = \mathbf{U}_i (\text{diag}(\lambda_1^i, \dots, \lambda_{r_i}^i))^{-1} (\mathbf{U}_i)^T \quad (102)$$

$$\tilde{\mathbf{L}}_i^0 = \tilde{\mathbf{U}}_i (\text{diag}(\tilde{\lambda}_1^i, \dots, \tilde{\lambda}_{\tilde{r}_i}^i))^{-1} (\tilde{\mathbf{U}}_i)^T. \quad (103)$$

To show this we first assume $\text{rank}(\mathbf{K}_{ij}) = N$ and take the right hand side of (96) and multiply it by $(\frac{1}{\sigma^2})^{r_{\mathbf{K}_{ij}}} (\sigma^2)^{r_{\mathbf{K}_{ij}}}$ to get

$$\left(\frac{1}{\sigma^2} \right)^{r_{\mathbf{K}_{ij}}} \left(|\mathbf{K}_{ij}| + (\sigma^2)^{r_{\mathbf{K}_{ij}}} (S_1 + \dots + S_{N-1}) \right). \quad (104)$$

Note now that for all S_m , $m = 1, \dots, N-1$, $\lim_{\sigma^2 \rightarrow 0} (\sigma^2)^{r_{\mathbf{K}_{ij}}} S_m = 0$. Therefore, (101) holds for the case $\text{rank}(\mathbf{K}_{ij}) = N$. To show the derivation of v_{ij} for the case $\text{rank}(\mathbf{K}_{ij}) < N$ we use the same technique where we multiply by $(\frac{1}{\sigma^2})^{r_{\mathbf{K}_{ij}}} (\sigma^2)^{r_{\mathbf{K}_{ij}}}$ the right hand side of (98) to get

$$\left(\frac{1}{\sigma^2} \right)^{r_{\mathbf{K}_{ij}}} \left((\sigma^2)^{r_{\mathbf{K}_{ij}}} S_{r_{\mathbf{K}_{ij}}} + (\sigma^2)^{r_{\mathbf{K}_{ij}}} \left(|\mathbf{L}_{ij}| + S_1 + \dots + S_{r_{\mathbf{K}_{ij}}-1} \right) \right). \quad (105)$$

As $\sigma^2 \rightarrow 0$ we can write $(\sigma^2)^{r_{\mathbf{K}_{ij}}} S_{r_{\mathbf{K}_{ij}}} = \text{pdet}(\mathbf{K}_{ij}) |(\mathbf{U}_{\mathbf{K}_{ij}}^\perp)^T \mathbf{L}_{ij}^0 \mathbf{U}_{\mathbf{K}_{ij}}^\perp|$. This concludes the derivation of (101). Note also that $v_{ij} > 0$, since the pseudo-determinant and the determinants in (101) are greater than zero.

Then, it follows immediately that the low-noise expansion of each term in the upper bound to the probability of error in (87) is given by

$$A_{ij} (\sigma^2)^{d_{ij}} + o \left((\sigma^2)^{d_{ij}} \right), \quad (106)$$

where

$$\begin{aligned} d_{ij} &= -\frac{\alpha_{ij}}{2} ((N - \tilde{r}_i) - (N - \tilde{r}_j)) \\ &\quad - \frac{1}{2}(N - r_i) - \frac{1}{2}(-\text{rank}(\mathbf{K}_{ij})) \\ &= \frac{1}{2}(\alpha_{ij}(\tilde{r}_j - \tilde{r}_i) + s_{ij}^V) \end{aligned} \quad (107)$$

$$A_{ij} = \left(\frac{\tilde{p}_j}{\tilde{p}_i} \right)^{\alpha_{ij}} \left(\frac{\tilde{v}_i}{\tilde{v}_j} \right)^{\frac{\alpha_{ij}}{2}} (v_i v_{ij})^{-\frac{1}{2}} > 0 \quad (108)$$

and

$$v_i = \text{pdet}(\Sigma_i) \quad (109)$$

$$\tilde{v}_i = \text{pdet}(\tilde{\Sigma}_i). \quad (110)$$

It therefore follows that the low-noise expansion of the upper bound to the probability of error in (87) is given by

$$\bar{P}(e) = A (\sigma^2)^d + o \left((\sigma^2)^d \right), \quad (111)$$

where

$$d = \min_{(i \neq j)} d_{ij} \quad (112)$$

and

$$A = \sum_{(i,j) \in \mathcal{S}_d} A_{ij}, \quad (113)$$

where $\mathcal{S}_d = \{(i,j) : d_{ij} = d\}$.

D. Proof of Corollary 2

Assume $s_{ij}^V > 0 \forall (i,j), i \neq j$ and

$$d_{\min}(\mathbf{U}_i, \tilde{\mathbf{U}}_i) < d_{\max}(\mathbf{U}_i, \tilde{\mathbf{U}}_j) \forall (i,j), i \neq j. \quad (114)$$

Note that

$$d_{\min}(\mathbf{U}_i, \tilde{\mathbf{U}}_i) < d_{\max}(\mathbf{U}_i, \tilde{\mathbf{U}}_j) \quad (115)$$

$$\implies \mathbf{U}_i^T (\tilde{\mathbf{U}}_i \tilde{\mathbf{U}}_i^T - \tilde{\mathbf{U}}_j \tilde{\mathbf{U}}_j^T) \mathbf{U}_i \succ \mathbf{0} \quad (116)$$

$$\implies \mathbf{U}_i^T (\tilde{\mathbf{U}}_{ij}' (\tilde{\mathbf{U}}_{ij}')^T - \tilde{\mathbf{U}}_{ji}' (\tilde{\mathbf{U}}_{ji}')^T) \mathbf{U}_i \succ \mathbf{0}, \quad (117)$$

where we have used results from the Appendix.

By taking $\mathbf{x} \in \mathbf{W}_{ij}$ or $\mathbf{x} \in \mathbf{V}_{ij}$ it is straightforward to show that (117) implies (16) and (17), thus obtaining conditions identical to those in Corollary 1.

E. Derivation of Example 1

We prove statement (33), by showing that

$$1 - \delta_{12} > N(\epsilon_1 + \epsilon_2) \quad (118)$$

together with $s_{12}, s_{21} > 0$ implies the sufficient conditions for perfect classification in Corollary 2.

Assume \mathbf{U}_i and \mathbf{U}_j are given and the singular values of $(\mathbf{U}_i)^T \mathbf{U}_j$ are known. We also know that $\tilde{\mathbf{U}}_j = \mathbf{Q}_j \mathbf{U}_j$. We can write

$$(\mathbf{U}_i)^T \tilde{\mathbf{U}}_j = (\mathbf{U}_i)^T \mathbf{U}_j + (\mathbf{U}_i)^T (\mathbf{Q}_j - \mathbf{I}) \mathbf{U}_j \quad (119)$$

On leveraging [35, Theorem 1], we can state that the i -th singular value \tilde{d}_i associated with $(\mathbf{U}_i)^T \tilde{\mathbf{U}}_j$ lies in the interval $[d_i - \|(\mathbf{U}_i)^T (\mathbf{Q}_j - \mathbf{I}) \mathbf{U}_j\|_2, d_i + \|(\mathbf{U}_i)^T (\mathbf{Q}_j - \mathbf{I}) \mathbf{U}_j\|_2]$, where d_i is the i -th singular value of $(\mathbf{U}_i)^T \mathbf{U}_j$. Then, we can write the upper bound

$$\|(\mathbf{U}_i)^T (\mathbf{Q}_j - \mathbf{I}) \mathbf{U}_j\|_2 \leq \|\mathbf{Q}_j - \mathbf{I}\|_2 = \epsilon_j \quad (120)$$

where the first inequality follows from the SVD separation theorem [36, Theorem 2.2]. Note also that

$$(\mathbf{U}_i)^T \tilde{\mathbf{U}}_i = \mathbf{I} + (\mathbf{U}_i)^T (\mathbf{Q}_i - \mathbf{I}) \mathbf{U}_i \quad (121)$$

where the singular values of $(\mathbf{U}_i)^T \tilde{\mathbf{U}}_i$ are bounded by $1 \pm \|(\mathbf{U}_i)^T (\mathbf{Q}_i - \mathbf{I}) \mathbf{U}_i\|_2$. By leveraging (120) we can further bound the singular values as $1 \pm \epsilon_i$.

Note now that

$$\begin{aligned} 1 - \delta_{12} &> (\epsilon_1 + \epsilon_2) \\ \iff \end{aligned} \quad (122)$$

$$\begin{aligned} 1 - \epsilon_1 &> \delta_{12} + \epsilon_2 \\ \iff \end{aligned} \quad (123)$$

$$1 - \epsilon_2 > \delta_{12} + \epsilon_1. \quad (124)$$

We now show that (123) implies

$$d_{\min}(\mathbf{U}_1, \tilde{\mathbf{U}}_1) < d_{\max}(\mathbf{U}_1, \tilde{\mathbf{U}}_2), \quad (125)$$

which is also equivalent to

$$\max_k \cos_k((\mathbf{U}_1)^T \tilde{\mathbf{U}}_2) < \min_l \cos_l((\mathbf{U}_1)^T \tilde{\mathbf{U}}_1), \quad (126)$$

where $\max_k \cos_k((\mathbf{U}_1)^T \tilde{\mathbf{U}}_2)$ denotes the cosine of the smallest principal angle between $\text{im}(\mathbf{U}_1)$ and $\text{im}(\tilde{\mathbf{U}}_2)$, $\max_k \cos_k((\mathbf{U}_1)^T \tilde{\mathbf{U}}_1)$ denotes the cosine of the largest principal angle between $\text{im}(\mathbf{U}_1)$ and $\text{im}(\tilde{\mathbf{U}}_1)$. The equivalence between (125) and (126) follows straight from the definition of min and max correlation distances. It is now easy to verify that (123) implies (126), since $1 - \epsilon_1$ is a lower bound for the cosine of the largest principal angles between \mathbf{U}_1 and $\tilde{\mathbf{U}}_1$, and $\delta_{12} + \epsilon_2$ is an upper bound to the cosine of the smallest principal angles between \mathbf{U}_1 and $\tilde{\mathbf{U}}_2$.

Finally, the same arguments can be used to show that (124) implies $d_{\min}(\mathbf{U}_2, \tilde{\mathbf{U}}_2) < d_{\max}(\mathbf{U}_2, \tilde{\mathbf{U}}_1)$. This concludes the proof.

REFERENCES

- [1] R. Duda, P. Hart, and D. Stork, *Pattern Classification (2nd Edition)*. New York, NY: Wiley-Interscience, 2000.
- [2] B. Frénay and M. Verleysen, "Classification in the Presence of Label Noise: a Survey," *IEEE Trans. Neural Networks Learn. Syst.*, vol. 25, no. 5, pp. 845–869, May 2014.
- [3] N. Natarajan, I. S. Dhillon, P. K. Ravikumar, and A. Tewari, "Learning with Noisy Labels," *Adv. Neural Inf. Process. Syst.* 26, pp. 1196–1204, 2013.
- [4] J. Bootkrajang and A. Kabán, "Label-noise Robust Logistic Regression and its Applications," in *Mach. Learn. Knowl. Discov. Databases*. Springer, 2012, vol. 7523, pp. 143–158.
- [5] J. Quiñonero-Candela, M. Sugiyama, A. Schwaighofer, and N. D. Lawrence, *Dataset Shift in Machine Learning*. The MIT Press, 2009.
- [6] R. Basri and D. W. Jacobs, "Lambertian Reflectance and Linear Subspaces," *IEEE Trans. Pattern Anal. Mach. Intell.*, vol. 25, no. 2, pp. 218–233, Feb. 2003.
- [7] K.-C. Lee, J. Ho, and D. Kriegman, "Acquiring Linear Subspaces for Face Recognition under Variable Lighting," *IEEE Trans. Pattern Anal. Mach. Intell.*, vol. 27, no. 5, pp. 684–698, May 2005.
- [8] J. Wright, A. Y. Yang, A. Ganesh, S. S. Sastry, and Y. Ma, "Robust Face Recognition via Sparse Representation," *IEEE Trans. Pattern Anal. Mach. Intell.*, vol. 31, no. 2, pp. 210–27, Feb. 2009.
- [9] Q. Zhang and B. Li, "Discriminative K-SVD for Dictionary Learning in Face Recognition," in *2010 IEEE Comput. Soc. Conf. Comput. Vis. Pattern Recognit.* IEEE, Jun. 2010, pp. 2691–2698.
- [10] E. Elhamifar and R. Vidal, "Sparse Subspace Clustering: Algorithm, Theory, and Applications," *IEEE Trans. Pattern Anal. Mach. Intell.*, vol. 35, no. 11, pp. 2765–2781, Nov. 2013.
- [11] C. Tomasi and T. Kanade, "Shape and Motion from Image Streams under Orthography: a Factorization Method," *Int. J. Comput. Vision, Springer*, vol. 9, no. 2, pp. 137–154, Nov. 1992.
- [12] T. E. Boult and L. G. Brown, "Factorization-based Segmentation of Motions," *Proc. IEEE Work. Vis. Motion*, 1991, pp. 179–186, Oct. 1991.
- [13] M. Chen, J. Silva, J. Paisley, C. Wang, D. Dunson, and L. Carin, "Compressive Sensing on Manifolds Using a Nonparametric Mixture of Factor Analyzers: Algorithm and Performance Bounds," *Signal Process. IEEE Trans.*, vol. 58, no. 12, pp. 6140–6155, 2010.
- [14] T. M. Cover and J. A. Thomas, *Elements of Information Theory*. John Wiley & Sons, 2012.
- [15] N. Merhav, G. Kaplan, A. Lapidot, and S. Shamai (Shitz), "On Information Rates for Mismatched Decoders," *IEEE Trans. Inf. Theory*, vol. 40, no. 6, pp. 1953–1967, Nov. 1994.
- [16] A. Lapidot and P. Narayan, "Reliable Communication Under Channel Uncertainty," *IEEE Trans. Inf. Theory*, vol. 44, no. 6, pp. 2148–2177, Oct. 1998.
- [17] A. Ganti, A. Lapidot, and I. E. Telatar, "Mismatched Decoding Revisited: General Alphabets, Channels with Memory, and the Wide-Band Limit," *IEEE Trans. Inf. Theory*, vol. 46, no. 7, pp. 2315–2328, Nov. 2000.
- [18] J. Scarlett, A. Martínez, and A. Guillen i Fabregas, "Mismatched Decoding: Error Exponents, Second-Order Rates and Saddlepoint Approximations," *IEEE Trans. Inf. Theory*, vol. 60, no. 5, pp. 2647–2666, May 2014.
- [19] A. Somekh-Baruch, "On Achievable Rates and Error Exponents for Channels With Mismatched Decoding," *IEEE Trans. Inf. Theory*, vol. 61, no. 2, pp. 727–740, Feb. 2015.
- [20] R. M. Gray and T. Linder, "Mismatch in High-Rate Entropy-Constrained Vector Quantization," *IEEE Trans. Inf. Theory*, vol. 49, no. 5, pp. 1204–1217, May 2003.
- [21] D. H. Chae, P. Sadeghi, and R. A. Kennedy, "Effects of Basis-mismatch in Compressive Sampling of Continuous Sinusoidal Signals," in *2010 2nd Int. Conf. Futur. Comput. Commun.*, vol. 2, 2010, pp. 739–743.
- [22] M. Herman and T. Strohmer, "General Deviants: An Analysis of Perturbations in Compressed Sensing," *IEEE J. Sel. Top. Signal Process.*, vol. 4, no. 2, pp. 342–349, Apr. 2010.
- [23] Y. Chi, L. L. Scharf, A. Pezeshki, and A. R. Calderbank, "Sensitivity to Basis Mismatch in Compressed Sensing," *IEEE Trans. Signal Process.*, vol. 59, no. 5, pp. 2182–2195, May 2011.
- [24] D. Kazakos, "Signal Detection under Mismatch (Corresp.)," *IEEE Trans. Inf. Theory*, vol. 28, no. 4, pp. 681–684, Jul. 1982.
- [25] R. Schlüter and H. Ney, "Model-Based MCE Bound to the True Bayes' Error," *IEEE Signal Process. Lett.*, vol. 8, no. 5, pp. 131–133, May 2001.
- [26] R. Schlüter, M. Nussbaum-Thom, E. Beck, T. Alkhouri, and H. Ney, "Novel Tight Classification Error Bounds under Mismatch Conditions based on \mathbb{S}^2 -Divergence," in *Inf. Theory Work. (ITW), 2013 IEEE*. IEEE, Sep. 2013, pp. 1–5.
- [27] S. Verdú, "Mismatched Estimation and Relative Entropy," *IEEE Trans. Inf. Theory*, vol. 56, no. 8, pp. 3712–3720, Aug. 2010.
- [28] G. H. Golub and C. F. Van Loan, *Matrix Computations (3rd Edition)*. Baltimore, MD: Johns Hopkins University Press, 1996.
- [29] J. Hamm and D. D. Lee, "Grassmann Discriminant Analysis: a Unifying View on Subspace-Based Learning," in *Proc. 25th Int. Conf. Mach. Learn.* ACM, 2008, pp. 376–383.
- [30] Q. Qiu and G. Sapiro, "Learning Transformations for Clustering and Classification," *ArXiv e-prints*, Sep. 2013.
- [31] R. Tron and R. Vidal, "A Benchmark for the Comparison of 3-D Motion Segmentation Algorithms," in *IEEE Conf. Comput. Vis. Pattern Recognit.*, Jun. 2007, pp. 1–8.
- [32] A. Galántai, "Subspaces, angles and pairs of orthogonal projections," *Linear Multilinear Algebr.*, vol. 56, no. 3, pp. 227–260, May 2008.
- [33] R. A. Horn and C. R. Johnson, *Matrix analysis*. Cambridge University Press, 2012.
- [34] I. Ipsen and R. Rehman, "Perturbation Bounds for Determinants and Characteristic Polynomials," *SIAM J. Matrix Anal. Appl.*, vol. 30, no. 2, pp. 762–776, Jul. 2008.
- [35] G. W. Stewart, "Perturbation Theory for the Singular Value Decomposition," *Tech. Rep. UMIACS-TR-90-124*, 1990.
- [36] C. Radhakrishna Rao, "Separation Theorems for Singular Values of Matrices and Their Applications in Multivariate Analysis," *J. Multivar. Anal.*, vol. 9, no. 3, pp. 362–377, Sep. 1979.